COMPARISON OF VIBRATIONAL ENERGY TRANSFER IN MICELLES AND VESICLES

By

Fredy Setiady Pratama

A THESIS

Submitted to
Michigan State University
In partial fulfillment of the requirements
for the degree of

Chemistry – Master of Science

2014

ABSTRACT

COMPARISON OF VIBRATIONAL ENERGY TRANSFER IN MICELLES AND VESICLES

By

Fredy Setiady Pratama

Understanding intermolecular energy transfer is important from both fundamental and applied perspectives. It is a process that determines thermal conductivity, an important property for applications such as cooling and lubrication. Our interest in vibrational energy transfer lies in the organization of fluid systems at the molecular level can influence the efficiency of vibrational energy transfer. We use one type of amphiphile that can for different assemblies in aqueous solution to determine how organization affects energy dissipation. Sodium decanoate was used as the amphiphile because it can form micelles or vesicles in aqueous solution, depending on the solution pH and the amphiphile concentration.

Our results provide evidence that micelles and vesicles affect the dissipation of vibrational energy. Vibrational population relaxation data show the time constant for intermolecular energy transfer from perylene to the amphiphile aliphatic chain differs by a factor of two for micelles and vesicles, and is more efficient in micelles. Complementary measurements of transient heating in these same systems show that micelles experience higher temperature change than vesicles following the deposition of excess energy into the system by means of internal conversion from the S_2 to S_1 states of perylene. This finding indicates that the non-specific dissipation of energy from the amphiphile assembly to the aqueous bath is the same to within the experimental uncertainty for vesicles and micelles. This finding is in contrast to our findings for mode-specific vibrational energy transfer and is likely a consequence of the non-mode-specific nature internal conversion within the chromophore.

ACKNOWLEDGMENTS

I would like to thank my advisor Dr. Gary Blanchard. He is an inspire figure in my life, a helpful, funny, and caring person. I'm going to miss his funny jokes during the group meeting and his magic during the alignment of the instrument. I have learned a lot from him from how to become a good chemist to how to become a professional person.

I would like to thank Dr. David Karpovich, Dr. Tamy Sivy, and Dr. Jason Pagano in Saginaw Valley State University (SVSU). They are very helpful during my undergraduate years and they love to guide their students to become good chemists.

I would like to thank my group members Stephen Baumler, Chen Qiu, Xiao Ran, Hannah Mize, Ke Ma, Krystyna Kijewski. Also the previous group member Dr. Doug Gornowich and Dr. Christine Ela Hay. It was a nice experience being in the group with them. It was fun to bug or annoy them.

I would like to thank my family and my girlfriend for their supports.

Also, I want to thank Huang's group for sharing their Dynamic Light Scattering instrument. They are very helpful when I needed help.

I would like to thank Dr. Kathy Severin for her help for teaching. She was very helpful and it was fun to be her teaching assistant.

Lastly, I want to thank National Science Foundation (NSF) for their funding on the instrument and American Chemical Society (ACS) Petroleum Research Fund (PRF) for their funding and for making this thesis possible.

TABLE OF CONTENTS

LIST OF TABLES

LIST OF FIGURES

Chapter 1: Introduction

1.1. The Motivation and the Importance of the Research

Understanding the process of energy transfer on the molecular scale is critical for solving thermal issues in molecular engineering applications (i.e. molecular electronics)[1-2] and for other applications where thermal conductivity needs to be controlled. To this day, the molecular details of thermal energy transfer remain to be understood fully.

The motivation for this research is to understand intermolecular vibrational energy transfer (VET). This process is the molecular scale basis for thermal conductivity. In nonmetals, thermal energy dissipation occurs primarily through transfer, led mainly though the vibrational and rotational energy transfer. This thesis focuses on intermolecular VET. The long term goal of this work is to understand the fundamental process of molecular scale vibrational energy transfer to provide the knowledge required to control thermal energy transfer properties. We focus on the initial details of VET and the effect of the organization of the immediate bath on that process. The second aim of this work is to understand the fate of the energy after its deposition into the system by monitoring non-mode specific transient heating in the system.

1.2. Molecular Vibrational Energy Transfer

During the dissipation of excess energy, both intramolecular and intermolecular energy transfer occurs. Intramolecular energy transfer is energy transfer within a molecule, where a high energy vibrational mode relaxes to lower energy vibrational modes. Intermolecular energy transfer is the transfer of energy from a vibrational excited molecule to different molecule. Intramolecular energy transfer is more prominent in low pressure gas phase than in the liquid phase due to the greater spacing between molecules in the gas phase.[3] For probe molecules in liquids, which is the

focus of this thesis, vibrational energy transfer between molecules is more significant because of the proximity of individual molecules.[4-5]

Intermolecular VET can occur collisionally (V-T, V-V, V-R) or by resonant energy transfer mediated by multipolar (e.g. dipole-dipole) coupling. Collisional energy transfer processes dominates in the gas phase and non-collisional energy transfer or resonant energy transfer dominates in the liquid phase.[3-4] In the work presented in this thesis, resonant energy transfer is the dominant process.

Before discussing the details of the findings regarding VET, it is important to consider the factors that influence the efficiency of resonant energy transfer from the donor molecule to the acceptor molecule. The factors which could affect this energy transfer process are the distance between the donor and acceptor molecules, the orientation of the donor with respect to the acceptor molecule, and the spectral overlap between the donor and acceptor. These factors are analogous to those in FRET (Fluorescence Resonant Energy Transfer), except VET involves vibration to vibration energy transfer that operates on a length scale of 10 Å or less,[6] while FRET involves coupling on length scales of 50 Å to 100 Å.[7] The rate of vibrational energy transfer depends on the details of the interaction between the donor and the acceptor. For the coupling between the vibrational mode of a donor molecule that is infrared (IR)-inactive and the Raman-active, and the vibrational mode of an acceptor that is IR-active, the coupling process is quadrupole-dipole in nature, with a characteristic distance dependence of r^{-8}.[8] The coupling between the vibrational mode of a donor that is IR active and the vibrational mode of an acceptor that is IR active scales as r^{-6}.[8] The higher the multipole moment, the shorter the intermolecular distance between the donor and acceptor required for energy transfer to occur. The strength of the coupling between the multipole moments of the donor and acceptor also depends on the relative orientation of the

two. This can be seen from the dipole-dipole interaction expression that was described by Förster,[7, 9-10]

$$k_{D\text{-}A} = \left(\frac{1}{\tau_D}\right)\frac{\left(0.529\left(N\kappa^2 n^{-4} Q_D J(\lambda)\right)\right)}{r^6} \qquad (1.1)$$

$k_{D\text{-}A}$ is the rate of donor-acceptor energy transfer, τ_D is the lifetime of the donor in the absence of the acceptor, κ is the factor describing the relative orientation between the donor and the acceptor, N is Avogadro's number, n is the refractive index, Q_D is the quantum yield of the donor in absence of acceptor, $J(\lambda)$ is the integral of the spectral overlap, r is the distance from the donor to the acceptor.[7, 9-10] Equation 1.1 shows that the energy transfer rate constant is proportional to κ^2. The higher the value for κ^2, the higher the rate of energy transfer. For dipole-dipole interaction, κ^2 is[11]

$$\kappa^2 = \left\{\sin\theta_D \sin\theta_A \cos\phi - 2\cos\theta_D \cos\theta_A\right\}^2 \qquad (1.2)$$

where θ_D is the donor dipole angle and θ_A is the acceptor angle with respect to the vector (r) connecting both donor and acceptor, and ϕ is the azimuthal angle between the donor and acceptor dipole moments (figure 1.1).

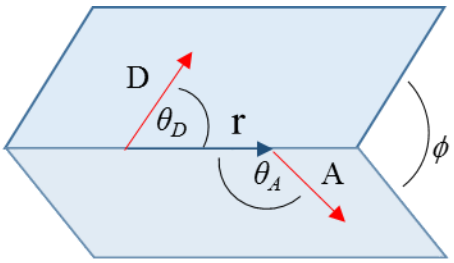

Figure 1.1. Relative Orientation of donor and acceptor.

For quadrupole-dipole interaction, κ^2 is[11]

$$\kappa^2 = \left\{\frac{3}{2}\left[\cos\theta_D\left(3\cos^2\theta_A - 1\right) - 2\sin\theta_D \sin\theta_A \cos\theta_A \cos\phi\right]\right\}^2 \qquad (1.3)$$

The term κ^2 has a range of 0 to 4. If the relative orientation of the multipole moments of the donor and acceptor is perpendicular ($\theta_A = 90°$, $\theta_D = 90°$, $\phi = 90°$ relative to vector r) κ^2 is zero for both types of interactions and VET will not occur. The κ^2 for other orientations will yield values above zero, thus VET will occur and its strength is dependent on the value of the κ^2 .[7]

Intermolecular energy transfer has been modeled using molecular dynamics (MD) simulations.[12-15] In addition to simulation, intermolecular VET has been examined experimentally.[4, 6, 16-22] These investigations were carried out using optical spectroscopic techniques. Optical spectroscopy can be performed in either the frequency domain or time domain. For homogeneously broadened vibrational bands, the linewidth ($\Delta\nu$) is related to the vibrational relaxation time (T) of that mode (equation 1.4).

$$\Delta\nu = \frac{1}{2\pi T} \tag{1.4}$$

$$\frac{1}{T} = \frac{1}{2T_1} + \frac{1}{T_2} \tag{1.5}$$

The time (T) which is observed for homogeneously broadened vibrational bands contains both vibrational population relaxation (T_1) and dephasing times (T_2) as shown in equation 1.5. Frequency domain spectroscopic techniques measures T only and it is not possible to separate the contribution from T_1 and T_2. Another problem is that vibrational bands in condensed phase systems are inhomogeneous broadened, giving rise more complication for T measurements. Unlike frequency domain measurements, time domain spectroscopic techniques have the ability to resolve T_1 and T_2 directly.[6, 16-18, 23-24]

The measurement of T_1 in the liquid phase can be done using picosecond or femtosecond spectroscopic methods. The picosecond spectroscopic methods are typically better suited for the measurement of intermolecular VET in room temperature liquids because the relevant vibrational

linewidths are a few cm^{-1}, well matched with the linewidth of ps pulses.[25] The timescale of this process is typically on the order of 10^{-11} s in the liquid phase.[6, 16-19] There are several methods capable of measuring VET in the liquid phase; with IR-Raman pump-probe spectroscopy[26-28] and stimulated emission pump-probe spectroscopy,[6, 16-18, 29] having been used extensively. In the following section, measurements of VET using stimulated emission pump-probe and IR-Raman pump-probe methods will be discussed.

1.3. VET Studies in The Liquid Phase IR-Raman Pump-Probe and Stimulated Emission Pump-Probe

Dlott's group has utilized IR-Raman pump-probe spectroscopy to measure intermolecular VET.[27] In one of their studies, they investigated VET between different sizes of alcohol (methanol, ethanol, and *t*-butyl alcohol) molecule and the NO_2 group of nitromethane to understand the vibrational relaxation dynamics of high explosives. They started by exciting the OH stretching vibration of the alcohol (3600 cm^{-1}) and monitoring the VET. They found VET began with intramolecular relaxation from the OH stretching mode to lower energy mode, CH stretching mode or CH bending mode, in the alcohol. The dominant intermolecular VET process is the transfer of energy from the CH bending mode (1402 cm^{-1}) of the alcohol to the symmetric NO_2 stretching mode of the nitromethane (1379 cm^{-1}). They found the three alcohols can function as the vibrational energy donor, though the efficiency of VET decreases as the molecular weight of alcohol increases due to the lower amplitude of CH bending motion in larger alcohols. The fact that many higher energy vibrational excitations (> 1600 cm^{-1}) that is followed by intramolecular relaxation to the CH bending mode is likely to undergo intermolecular VET efficiently to NO_2 suggests that NO_2 is prevalent in secondary explosions.[27]

Another study that was done by the Dlott's group using the IR-Raman pump-probe technique is the measurement of vibrational energy transfer across a reverse micelle layer.[26] In this case, the flow of vibrational energy between bulk water and bulk CCl_4 is separated by a sodium dioctyl sulfosuccinate (AOT) monolayer interface is monitored. The water molecules were in the core of the reverse micelles, which are surrounded by bulk CCl_4 liquid. When the water OH stretching mode is excited, the time required for vibrational energy to transfer from the water to the polar head group of the AOT amphiphile was ca. 1.8 ps and 10 ps for the vibrational energy to transfer out to the bulk CCl_4. When the aliphatic chain of the AOT amphiphile (methyl stretching mode) is excited, even though it is in close physical proximity to the bulk CCl_4, the energy transfer required ~ 40 ps to transfer from the aliphatic chain of the AOT amphiphile to the bulk CCl_4. This finding indicated that the energy transfer pathway through the micelle is largely dependent on specific vibrational couplings.[26]

There are several experimental reports using the stimulated emission pump-probe method on VET in homogeneous environments and heterogeneous environments. Jiang et. al. have measured the VET from perylene to the surrounding bath in different chain length of alkane solution to understand the solute solvent interactions.[6] In that study, the T_1 of the perylene ring breathing mode (1375 cm^{-1}) which is degenerate with the terminal methyl rocking mode (1378 cm^{-1}) of the alkane solvent was measured as a function of alkane chain length. That study showed the dominant energy transfer from solute to solvent is mediated by resonant energy transfer rather than collisional energy transfer.

Another study in which VET measurements were carried out was perylene and 1-methylperylene in alkanols.[16] In that study, the ring breathing modes of perylene and 1-methylperylene were investigated as a function of solvent alcohol chain length. Perylene possesses

center of inversion, where 1-methylperylene does not possess center of inversion. The experimental data show that the vibrational energy couplings between the donor ring breathing mode and the acceptor terminal methyl rocking mode are more efficient in 1-methylperylene than in perylene. This is expected because the coupling between the 1-methylperylene ring breathing mode (IR and Raman-active) and the alcohol terminal methyl rocking mode (IR-active) is dipole-dipole where the distance dependence of VET scales as r^{-6}. The coupling between the perylene ring breathing mode (Raman-active and IR-inactive) and the alcohol terminal methyl rocking mode (IR-active) is quodrupole-dipole, with a characteristic distance dependence of r^{-8}.[16] These differences in the distance-dependence of the two energy transfer processes, are seen in the results for the two donors.

Qiu et. al. have measured VET in heterogeneous systems using stimulated emission pump-probe spectroscopy.[29] They studied the VET of perylene in the binary solvent mixture of cyclohexane and ethanol to relate the solvent system composition to the local organization.[29] In that study, the concentration of ethanol relative to that of cyclohexane was varied. The mode which was investigated was the ring breathing mode of perylene which is degenerate with the methyl rocking mode of ethanol. The results of this work show a discontinuity in T_1 between the mixture of 5.0% ethanol in cyclohexane and 7.5% ethanol in cyclohexane. At 7.5% ethanol or above, the T_1 time constant of the ring breathing mode of the perylene is distinctly shorter than for 5.0% or less ethanol, by a factor of 5. This finding suggests that the distance between perylene and ethanol is shorter by ~ 1 Å in $\geq$ 7.5 % ethanol in cyclohexane than in $\leq$ 5.0 % ethanol in cyclohexane. The fact that T_1 is a factor of 5 different for $\geq$ 7.5 % ethanol in cyclohexane suggests that other factors such as relative orientation of perylene to ethanol, plays an important role in mediating.

1.4. Background of the System Studied in This Research

In this thesis, we are interested in understanding how different local organization can affect energy flow on the molecular scale. One way to achieve this understanding is by measuring VET from perylene in a solution containing alkanoate amphiphiles.

The benefit of using alkanoate amphiphiles lies in their ability to form different structures that are characterized by different local organization. One way to control the local environment is by adjusting the pH of the solution. Above the critical micelle concentration (cmc), micelles (figure 1.2a) will form when the pH of the aqueous solution is high.[30-31] Above the critical vesicle concentration (cvc), vesicles (figure 1.2b) will form when the pH of the solution is near neutral.[31-33]

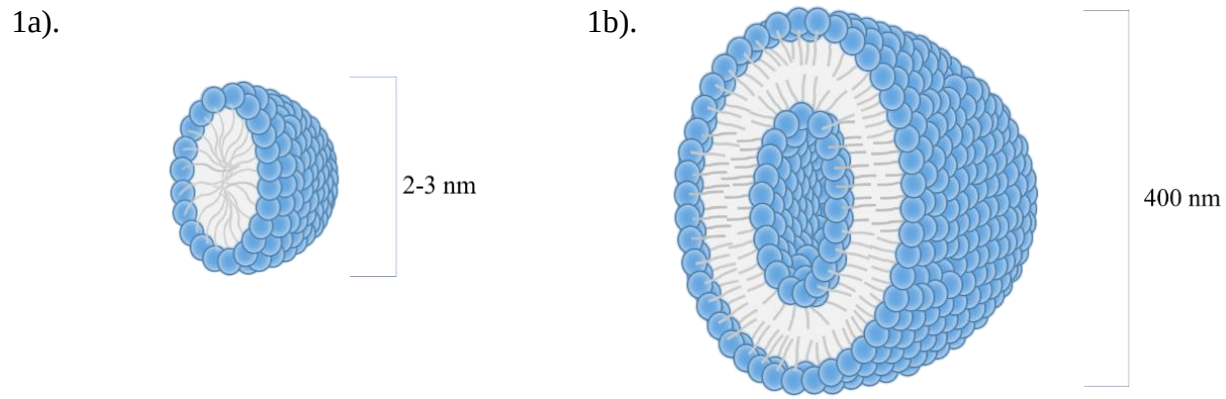

Figure 1.2. Structure of a) micelle and b) vesicle.

For micelles in aqueous solution, the amphiphile aggregates have a hydrophobic core and the polar head groups face out to interact with the solvent.[34] In contrast, vesicles are amphiphile bilayer structures that close on themselves. These two structural motifs have different curvature, with micelles having a much smaller radius than vesicles. Another way to create different local environments is by adjusting the size of vesicles using membranes with different pore sizes during vesicle extrusion. As the diameter of vesicles increases, the local environment within vesicles and

aliphatic chain region become closer to planar. For this thesis, we controlled the local organization of the environment by adjusting the pH of the solution.

In this work, sodium decanoate (figure 1.3a) was used because it is readily soluble in water and decanoate micelles and decanoate / decanoic acid (figure 1.3b) vesicles have been studied extensively.[31-32, 35-37] The formation of micelles or vesicles depends on the charge on the head groups of the amphiphiles.[38] For micelles to form, the head groups of the amphiphiles need to be deprotonated. This causes the charge repulsion between the head groups of the amphiphiles. When some of the amphiphiles are protonated and some are deprotonated, the charge repulsion of the amphiphile head groups' is less extensive, allowing for the formation of vesicles.[32-33, 39-40] Spherical decanoate micelles will form when the solution pH is high (above pH 8.5) and the concentration of the decanoate is at 50 mM (cmc) or above.[31] Decanoate / decanoic acid vesicle will form when the concentration of decanoate / decanoic acid is 20 mM (cvc) or above and the solution pH is in the range 6.4 - 7.8.[31] It is important to note that the pK_a of decanoic acid is ≈ 4.9 and that vesicles is usually form near the pK_a.[31] The differences in pK_a and pH of vesicle formation is caused by the variation between the pH of the polyanionic vesicle surface and the pH of the bulk solution.[31, 41-42] Past studies have shown that the negative charge surface of the membrane attracts protons from the bulk leading to higher pH in the bulk solution and lower pH at the surface of the membrane. The bulk pH can be up to 3 units higher than the pH of the vesicle surface.[42] The intrinsic pK_a of the decanoic acid is the 4.9 if the influence of the surface is neglected.[41]

In order to investigate energy transfer in micelles and vesicles, a probe molecule is used. The probe molecule serves as the site of energy deposition, from which energy is dissipated nonradiatively to its local environment. For this work, a polycyclic aromatic hydrocarbon (PAH) probe is used because it is a nonpolar molecule which partitions selectively into the nonpolar

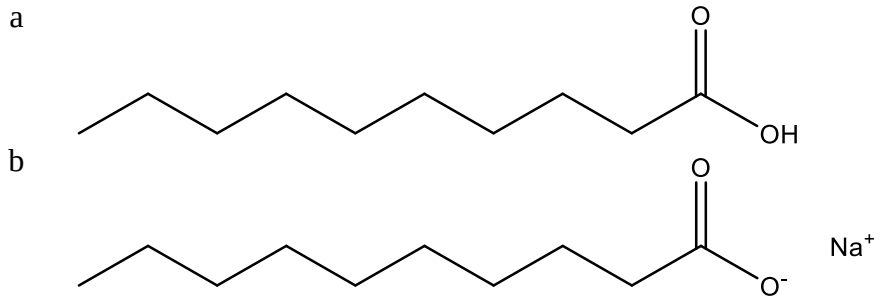

Figure 1.3. Structure of a) Decanoic Acid and b) Sodium Decanoate.

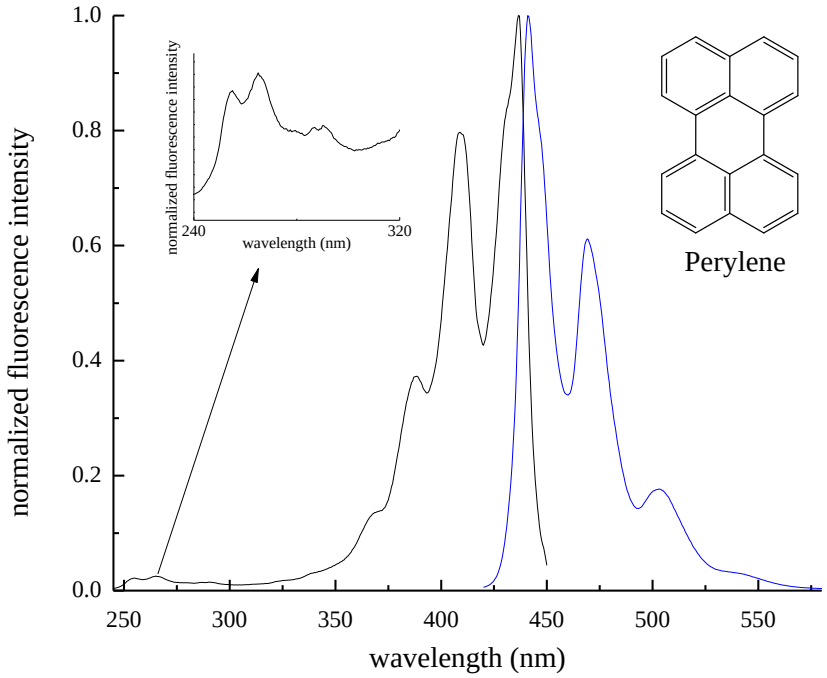

Figure 1.4. Structure of perylene (top right) and excitation (black) and emission (blue) spectra of perylene in decanoate micelles. Inlet figure: Expanded scale for the excitation peaks in UV region.

regions of micelles or vesicles. Perylene (figure 1.3), which D_2h point group symmetry, was chosen as the probe molecule because it has been studied,[4, 6, 16-17] has a high fluorescence quantum yield ($\Phi \approx 0.94$)[43], and its insolubility in water. It is not known at this point whether perylene is located in the core or the aliphatic chain region of micelle. For perylene in vesicles, previous studies showed that the location of perylene in 1,2-dimyristoyl-*sn*-glycero-3-phosphocholine (DMPC) lipid vesicles is in the acyl chain region of one of the vesicle leaflets for vesicles with diameters less than 800 nm. For larger diameter vesicles, perylene resides in the inter-leaflet gallery.[44] For the work presented in this thesis, 400 nm diameter vesicles were used. While internal structure is different for decanoate / decanoic acid vesicles than for DMPC vesicles, the location of perylene is largely dependent on the curvature, and we believe the probe to be housed in the aliphatic chain length.

Two separate investigations were carried out in order to gain an understanding of energy transfer from perylene in micelles and vesicles to the surrounding bath. The first investigation is to monitor the initial energy transfer from perylene using stimulated emission pump-probe measurements (mode specific information) and the second investigation is to monitor the results of energy transfer into the bath by transient heating measurements (non-mode specific easurement) using time-correlated single photon counting (TCSPC) detection of the probe emission for two different excitation conditions.

The pump-probe instrument that is used measures the stimulated emission from the probe that contains information on the population relaxation time (T_1) of the perylene ring breathing mode (1375 cm^{-1}) in decanoate micelles or decanaote / decanoic acid vesicles. The benefit of using this technique is it can selectively excite a specific vibrational mode of the probe in the presence of a degenerate bath mode, and one can monitor direct vibrational energy transfer from

perylene to decanaote or decanoic acid. IR pump-probe measurements excite both donor and acceptor vibrational modes when they are degenerate, precluding measurement of direct vibrational energy transfer when the energy of the donor and the bath acceptor modes are degenerate.

For T_1 measurements, the vibrational mode we monitored is the perylene ring breathing (1375 cm^{-1}, Raman active and IR inactive) because it is degenerate with the rocking mode (1378 cm^{-1}, IR active) of the terminal methyl group of the amphiphiles. The perylene symmetric ring breathing mode modulates the molecular quadrupole moment, while the terminal methyl group rocking mode is dipole active. Because the donor-acceptor coupling is quadrupole-dipole, the rate of energy transfer scales with r^{-8}.[8] The details of this result will be described in chapter 3.

To complement the T_1 measurements, transient heating measurements were performed. The transient heating measurement senses the average temperature change ($\boldsymbol{\Delta T}$) of the local environment, average over the timescale of the chromophore reorientation in decanoate micelles or decanoate / decanoic acid vesicles. To perform this measurement, two different anisotropy decay measurements were carried out for two different initial excitation conditions. One anisotropy decay measurement involves excitation of the perylene from ground state to the S_1 electronic state ($S_1 \leftarrow S_0$) and the other involves excitation from the ground state to the S_2 electronic state ($S_2 \leftarrow S_0$). Both of these excitations result in photon emission from the relaxation of the S_1 electronic state to the ground according to Kasha's rule.[45] Because relaxation from S_2 to S_1 is nonradiative[45] ($\approx$ 1.98 eV), the anisotropy decay from both excitation conditions are expected to be different, with the anisotropy decay associated with $S_1 \leftarrow S_0$ excitation being slower than that seen for $S_2 \leftarrow S_0$ excitation. Because the $S_2 \leftarrow S_0$ energy is dissipated into the local environment, it is expected that the perylene anisotropy decay seen for $S_2 \leftarrow S_0$ excitation will be faster due to transient heating.

Previous transient heating measurements performed using perylene in DMPC vesicles, tetracene in n-alkanes, and Rhodamine 640 in alcohols, provide sound precedent.[46-49] Transient heating measurements of perylene in decanoate micelles and decanoate / decanoic acid vesicles exhibit faster anisotropy for $S_2 \leftarrow S_0$ excitation than $S_1 \leftarrow S_0$ excitation. The data represented in this thesis provide evidence that energy is dissipated differently in micelles and vesicles.

Chapter 2 of this dissertation describes the preparation of decanoate micelles and decanoate / decanoic acid vesicles, the stimulated emission pump-probe instrument and TCSPC instrument, and briefly describes the dynamic light scattering (DLS) instrument.

Chapter 3 of this dissertation discusses the findings of the vibrational population relaxation dynamics of the perylene ring breathing mode and the transient heating of the chromophore local environment in decanoate micelles and decanoate / decanoic acid vesicles. Thermal energy is dissipated differently in decanoate micelles and in decanoate / decanoic acid vesicles.

Chapter 4 of this dissertation provides the final conclusion and suggestions for future studies.

REFERENCES

REFERENCES

1. Jortner, J.; Nitzan, A.; Ratner, M., Foundations of Molecular Electronics – Charge Transport in Molecular Conduction Junctions. In *Introducing Molecular Electronics*, Cuniberti, G.; Richter, K.; Fagas, G., Eds. Springer Berlin Heidelberg: 2005; Vol. 680, pp 13-54.

2. Segal, D.; Nitzan, A.; Hänggi, P. *The Journal of Chemical Physics* **2003,** *119* (13), 6840-6855.

3. Yardley, J. T., *Introduction to Molecular Energy Transfer*. Academic Press: New York, 1980.

4. Jiang, Y.; Blanchard, G. J. *The Journal of Physical Chemistry* **1994,** *98* (38), 9417-9421.

5. Jiang, Y.; Hambir, S. A.; Blanchard, G. J. *Optics Communications* **1993,** *99* (3–4), 216-220.

6. Jiang, Y.; Blanchard, G. J. *The Journal of Physical Chemistry* **1994,** *98* (38), 9411-9416.

7. Clegg, R. M., Chapter 1 Förster resonance energy transfer-FRET what is it, why do it, and how it's done. In *Laboratory Techniques in Biochemistry and Molecular Biology*, 2009; Vol. 33, pp 1-57.

8. Gray, C. G.; Gubbins, K. E., *Theory of Molecular Fluids/ Vol. 1, Fundamentals*. Oxford : Clerendon Press 1984: New York, 1984.

9. Förster, T. *Annalen der Physik* **1948,** *437* (1-2), 55-75.

10. Lakowicz, J. R., *Principles of Fluorescence Spectroscopy*. 3rd ed.; Springer US: New York, 2006.

11. Rigby, M., *The Forces between molecules*. Clarendon Press: 1986.

12. Ohara, T. *The Journal of Chemical Physics* **1999,** *111* (14), 6492-6500.

13. Ohara, T. *The Journal of Chemical Physics* **1999,** *111* (21), 9667-9672.

14. Ohara, T.; Chia Yuan, T.; Torii, D.; Kikugawa, G.; Kosugi, N. *The Journal of Chemical Physics* **2011,** *135* (3), -.

15. Nakano, T.; Kikugawa, G.; Ohara, T. *The Journal of Chemical Physics* **2010,** *133* (15), -.

16. Goldie, S. N.; Blanchard, G. J. *The Journal of Physical Chemistry A* **1999,** *103* (8), 999-1006.

17. Goldie, S. N.; Blanchard, G. J. *The Journal of Physical Chemistry A* **2001,** *105* (28), 6785-6793.

18. Jiang, Y.; Blanchard, G. J. *The Journal of Physical Chemistry* **1995,** *99* (20), 7904-7912.

19. McCarthy, P. K.; Blanchard, G. J. *The Journal of Physical Chemistry* **1995,** *99* (50), 17748-17753.

20. McCarthy, P. K.; Blanchard, G. J. *The Journal of Physical Chemistry* **1996,** *100* (13), 5182-5187.

21. Qiu, C.; Blanchard, G. J. *The Journal of Physical Chemistry B* **2014,** *118* (35), 10525-10533.

22. McCarthy, P. K.; Blanchard, G. J. *The Journal of Physical Chemistry* **1996,** *100* (35), 14592-14597.

23. Zinth, W.; Kolmeder, C.; Benna, B.; Irgens-Defregger, A.; Fischer, S. F.; Kaiser, W. *The Journal of Chemical Physics* **1983,** *78* (6), 3916-3921.

24. Kel, O.; Tamimi, A.; Fayer, M. D. *Proceedings of the National Academy of Sciences* **2014,** *111* (3), 918-923.

25. Blanchard, G. J. *Analytical Chemistry* **1997,** *69* (11), 351A-357A.

26. Deàk, J. C.; Pang, Y.; Sechler, T. D.; Wang, Z.; Dlott, D. D. *Science* **2004,** *306* (5695), 473-476.

27. Hong, X.; Chen, S.; Dlott, D. D. *The Journal of Physical Chemistry* **1995,** *99* (22), 9102-9109.

28. Laubereau, A.; Kaiser, W. *Reviews of Modern Physics* **1978,** *50* (3), 607-665.

29. Qiu, C.; Blanchard, G. J. *The Journal of Physical Chemistry B* **2014**.

30. McBain, J. W.; Salmon, C. S. *Journal of the American Chemical Society* **1920,** *42* (3), 426-460.

31. Namani, T.; Walde, P. *Langmuir* **2005,** *21* (14), 6210-6219.

32. Morigaki, K.; Walde, P.; Misran, M.; Robinson, B. H. *Colloids and Surfaces A: Physicochemical and Engineering Aspects* **2003,** *213* (1), 37-44.

33. Cistola, D. P.; Atkinson, D.; Hamilton, J. A.; Small, D. M. *Biochemistry* **1986,** *25* (10), 2804-2812.

34. Voet, D. J.; Voet, J. G.; Pratt, C. W., *Principles of Biochemistry*. John Wiley & Sons, Inc: Hoboken, NJ, 2008.

35. Stevenson, S. A.; Blanchard, G. J. *The Journal of Physical Chemistry B* **2006,** *110* (26), 13005-13010.

36. Dejanović, B.; Mirosavljević, K.; Noethig-Laslo, V.; Pečar, S.; Šentjurc, M.; Walde, P. *Chemistry and Physics of Lipids* **2008,** *156* (1–2), 17-25.

37. Maher, S.; Leonard, T. W.; Jacobsen, J.; Brayden, D. J. *Advanced Drug Delivery Reviews* **2009,** *61* (15), 1427-1449.

38. Israelachvili, J. N.; Mitchell, D. J.; Ninham, B. W. *Journal of the Chemical Society, Faraday Transactions 2: Molecular and Chemical Physics* **1976,** *72* (0), 1525-1568.

39. Cistola, D. P.; Hamilton, J. A.; Jackson, D.; Small, D. M. *Biochemistry* **1988,** *27* (6), 1881-1888.

40. Apel, C. L.; Deamer, D. W.; Mautner, M. N. *Biochimica et Biophysica Acta (BBA) - Biomembranes* **2002,** *1559* (1), 1-9.

41. Haines, T. H. *Proceedings of the National Academy of Sciences* **1983,** *80* (1), 160-164.

42. Gebicki, J. M.; Hicks, M. *Chemistry and Physics of Lipids* **1976,** *16* (2), 142-160.

43. Berlman, I. B., *Handbook of Fluorescence Spectra of Aromatic Molecules*. 2nd ed.; Academic Press: New York, 1971.

44. Lapinski, M. M.; Blanchard, G. J. *Chemistry and Physics of Lipids* **2008,** *153* (2), 130-137.

45. Kasha, M. *Discussions of the Faraday Society* **1950,** *9* (0), 14-19.

46. Dela Cruz, J. L.; Blanchard, G. J. *The Journal of Physical Chemistry A* **2001,** *105* (41), 9328-9335.

47. Pillman, H. A.; Blanchard, G. J. *The Journal of Physical Chemistry B* **2010,** *114* (43), 13703-13709.

48. Pillman, H. A.; Blanchard, G. J. *The Journal of Physical Chemistry B* **2011,** *115* (14), 3819-3827.

49. Mize, H. E.; Blanchard, G. J. *The Journal of Physical Chemistry B* **2013,** *117* (50), 16260-16265.

Chapter 2: Experimentation and Instrumentation

2.1. Steady State Measurement and Sample Preparation.

2.1.1. Steady State Spectroscopy. The steady state excitation and emission spectra of perylene in decanoate micelles and decanoate / decanoic acid vesicles were recorded using a Jobin-Yvon Spex Fluorolog 3 instrument. The spectral resolution for all measurements was set to 1.0 nm for both excitation and emission monochromators. Excitation and emission spectra reported here are the averages of ten scans. Spectra of perylene in vesicles were corrected for scattering by subtraction of a blank solution containing vesicles but not perylene. Calibration curve measurements were carried out by exciting at 410 nm for perylene in micelle-containing solution and vesicle containing solution and monitoring the emission intensity at 470 nm for vesicle-containing solution and 469 nm for micelle containing solution.

2.1.2. Chemicals. Perylene (Sigma Aldrich, 99%), sodium decanoate (TCI, 99%), sodium monobasic phosphate (J. T. Baker, 99%) sodium dibasic phosphate (Fluka, 99%), hydrochloric acid (CCI) were used as received, without further purification. The perylene stock solution used for addition to micelle and vesicle forming solutions was $1x10^{-4}$ M in ethanol (distilled in-house).

2.1.3. Micelle-containing solutions. Sodium decanoate is dissolved in 100 mM, pH 10.3 sodium phosphate buffer to produce a 400 mM decanoate solution. Ethanolic perylene solution is dried by a N_2 stream and taken up in the decanoate-containing solution to produce an overall perylene concentration of $4x10^{-5}$ M if all were dissolved in the solution. The solution was stirred overnight then filtered using 0.2 μm pore diameter syringe filter (Whatman). The calibration curve was generated using steady state measurements to determine the amount of perylene that was solubilized when the solution was mixed by stirring overnight (figure 2.1). The perylene containing micelle solution standards were prepare using five cycles of freeze-thaw-vortex mixing

to ensure perylene dissolves in the micelle solution. The final concentration of perylene solubilized in the micelles was determined to be ≈ 6.0 ± 0.5 μM.

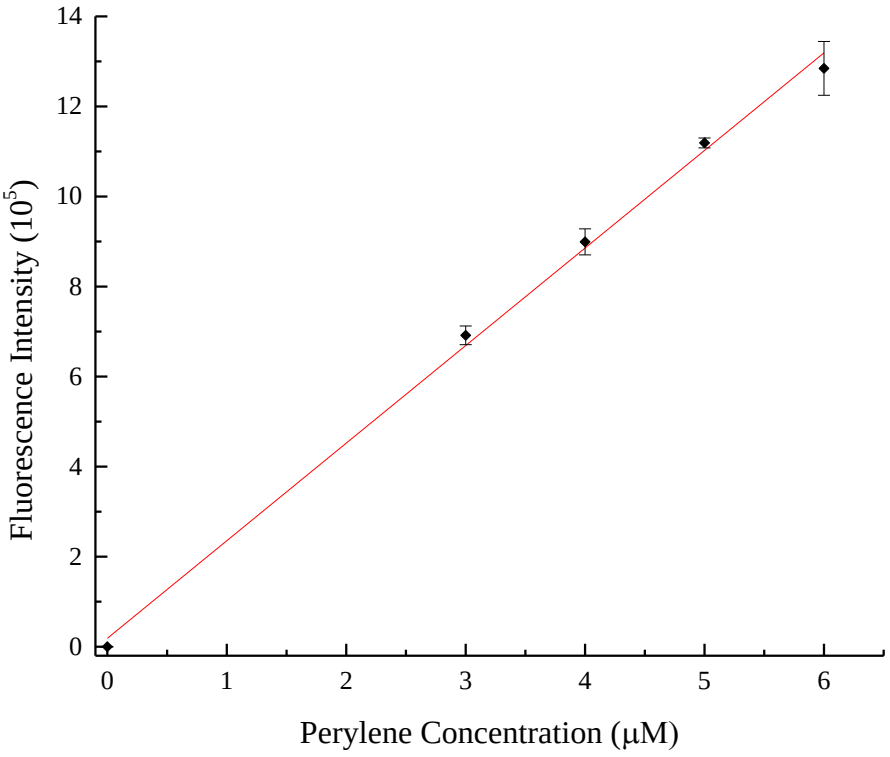

Figure 2.1. Calibration curve of perylene in decanoate micelle-containing solution.

2.1.4. Vesicle-containing solutions. Sodium decanoate was added to a sodium phosphate (100 mM, pH 6.8) buffer solution. The analytical concentration of sodium decanoate was 400 mM and 200 mM for HCl. The pH of the resulting solution was 7.2 ± 0.1 (Orion Research ionanalyzer/501). Perylene in ethanol solution was dried under a N_2 stream and taken up in the buffered decanoate / decanoic acid solution. Five freeze-thaw-vortex cycles were performed on the solution to ensure mixing of the constituents. For each cycle the solution was frozen using $N_2(l)$ for 5 minutes, thawed by immersion in a 60 °C water bath for 5 minutes, and vortexed for 2 minutes. The solution was then extruded using a mini-extruder system (Avanti Polar Lipids) and

polycarbonate filter with 400 nm diameter pores (Whatman). The calibration curve (r^2 =0.9976) was generated to determine the maximum concentration of perylene in vesicle-containing solutions when mixing using the freeze-thaw-vortex method (figure 2.2). To ensure that 6 μM perylene can be dissolve in vesicle-containing solutions, a calibration curve range from 4 μM to 7 μM was constructed. Because the 6 μM data point is linear with the rest of the concentration, it confirms that perylene at that concentration was all dissolved.

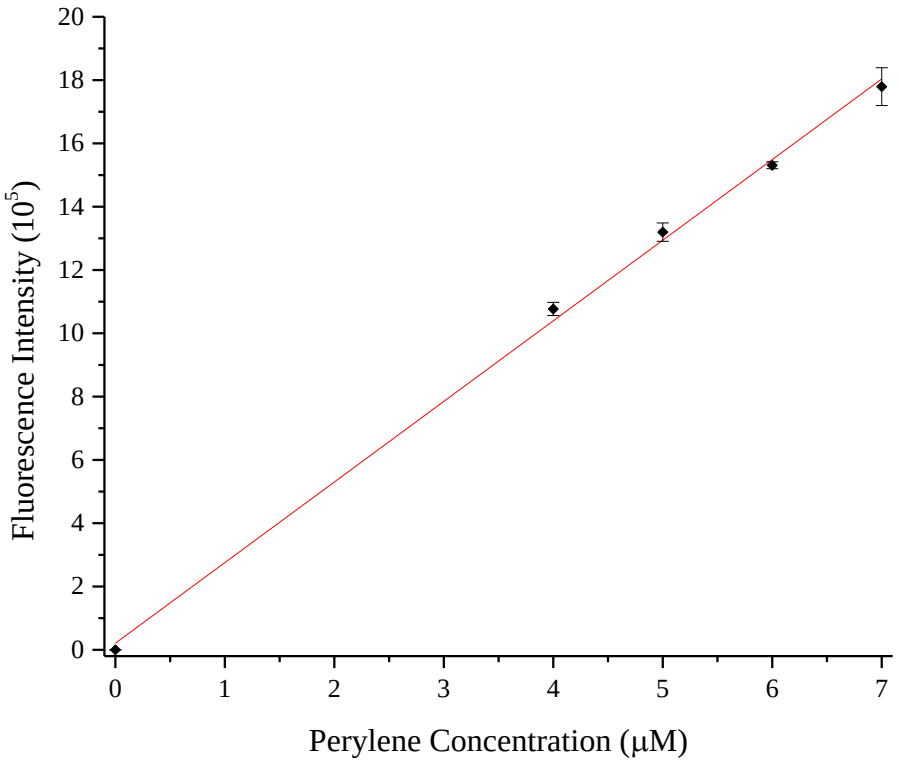

Figure 2.2. Calibration curve of perylene in decanaote/ decanoic acid vesicle-containing solution.

2.2. Pump-Probe Spectrometer

This section discusses the instrument that was used to measure vibrational population relaxation, T_1, of perylene in decanoate micelles or decanoate / decanoic acid vesicles is stimulated emission pump-probe system is shown in figure 2.3. The instrument employs both "pump" and

"probe" pulses, where the pump pulse is used to excite perylene to the electronic excited state ($S_1^{v=0}$) and the probe pulse is used to stimulate emission from the $S_1^{v=0}$ to $S_0^{v=1}$ state and monitor the T_1 relaxationof perylene in micelles or vesicles. This instrument was set up to measure samples in solution and its schematic is similar to an earlier version of the instrument operated by the Blanchard group.[1-3] The current instrument has several advantages, including higher laser stability and shorter instrument response function due to the shorter laser pulses used. Described below are, the details of the components as well as the signal detected.

2.2.1. Light Source. For the measurement of vibrational energy transfer, picosecond laser pulses are chosen rather than femtosecond pulses because the linewidth of molecular vibrational bands is 20 cm^{-1} or less, which corresponds to ~ 1.7 picoseconds from the Fourier relationship between the time and frequency domains.[4] The source laser for this instrument is a passively mode locked Nd: YVO_4 diode pumped laser (Spectra Physics Vanguard). It has an output of a train of 13 ps pulses separated in time by 12.5 ns. It produces the second harmonic (532 nm) and third harmonic (355 nm) of the fundamental wavelength (1064 nm) with average power of 2.5 W at each harmonic. For the work in this thesis, we used the 355 nm output to synchronously pump two cavity-dumped dye lasers (Coherent 702-3 dye lasers, Gooch and Housego cavity dumping electronics). Both dye lasers were operated with Stilbene 420 dye (Exciton). The output of the dye lasers are 5 ps pulses with the repetition rate set at 8 MHz (125 ns between pulses) and 100 mW average power. For the work reported in this thesis, we set the pump laser at the wavelength that corresponds with the 0-0 transition of perylene (438.8 nm for micelles and 440.2 nm for vesicles) and the probe laser at the wavelength that corresponds to the frequency lower than the pump by 1375 cm^{-1} (467.0 nm for micelles and 468.8 nm for vesicles).

The output of the dye laser is characterized by flicker noise that is associated with the

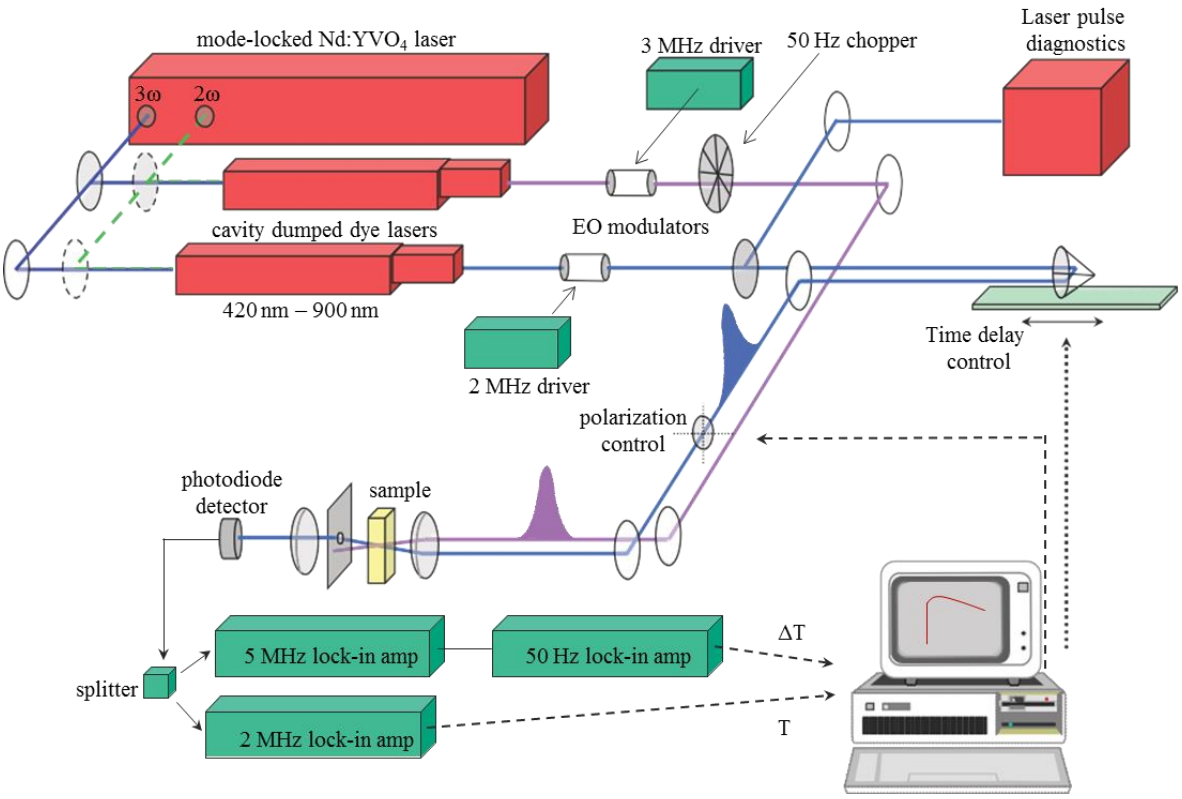

Figure 2.3. Pump-probe instrument schematic.

flowing of the dye solution through the jet nozzle. With an experimental signal size of $\Delta T/T \approx 10^{-4}$ (ΔT = transmitted signal intensity, T = transmitted probe intensity) or less which is at least two orders of magnitude less than the flicker noise, the experimental signal will not be detected. To solve that problem, we employed a three modulation signal encoding and detection scheme.

2.2.2. Modulation. We use a three modulation signal encoding and detection scheme to shift the signal carrier frequency to a region of the dye laser output spectrum characterized by a shot noise limited floor.[5-7] The noise spectrum of the dye lasers scales as $1/f$, reaching the shot noise regime at frequencies above 1 MHz.[5] We employed electro-optic modulators (Thorlab, model: GTH5M) to amplitude modulate the laser pulse trains at frequencies greater than 1 MHz. Both pump and probe pulses are modulated at different frequencies and the resulting signal frequency is generated at the sum and difference of the beam modulation frequencies.

$$\cos \omega_1 \times \cos \omega_2 = \frac{1}{2}\cos (\omega_1 + \omega_2) + \frac{1}{2}\cos(\omega_1 - \omega_2) \quad (2.1)$$

where ω_1 is the pump laser amplitude modulation frequency (3 MHz) and ω_2 is the probe laser amplitude modulation frequency (2 MHz). Along with the electro-optic modulators, a mechanical chopper (HMS, 220A) set to a frequency of 50 Hz was also applied to the pump pulse train to avoid the detection of electronic broadcast artifact and nonlinear frequency mixing effects in the photodiode detector. The signal demodulation was performed radio frequency lock-in amplifier (Stanford Research Systems, SR844) and an audio frequency lock-in amplifier (Stanford Research Systems, SR510). For this instrument, the experimental signal at 5 MHz $\pm$ 50 Hz frequency is detected and the probe intensity, T, is acquired by demodulation of the probe signal at 2 MHz. The final sensitivity of this instrument is $\Delta T/T \approx 10^{-7}$.[8]

The measurement of T_1 was done at the magic angle to eliminate contributions from the signal associated with molecular motion. This was done by setting the probe laser polarization to 54.7° relative to the pump laser polarization (0°) using a polarization controller (Newport, PR-550). To control the temporal relationship between the pump and probe pulses, the pump pulse beam path is fixed while the probe pulse pathlength is varied using a broadband corner-cube reto-reflector (Newport, UBR 2.5-1) that is equipped with using a translation stage (Parker Daedal, 110708 R0175). This translation stage controls the arrival time (1 ps resolution) of probe pulse relative to the pump pulse at the sample. Both pulses are focused to the same point in the sample. To minimize thermal lensing effects, the sample was placed in a flow cell and a pump was used to flow the sample through the cell using a closed loop, temperature controlled system. The probe pulse train, which carries the information of interest, was detected using photodiode detector (RCA C30956E). The acquired signal is of the form $\Delta T/T$ as a function of time. For the works presented

on this thesis, the time window per scan is 700 ps. Approximately 60 scans were collected per sample measurement and triplicate measurements were performed.

2.2.3. Overall Signal. The experimental signal can be explained by treating the chromophore as a coupled three level system shown in figure 2.4a. Absorption and stimulated emission occur for both pump and probe pulses, and they contribute to the overall form of the detected signal in different ways. The information that is detected on the probe beam includes the population difference between the in $S_1^{v=0}$ and $S_0^{v=v}$ states.

The details of how absorption and stimulated emission affect the overall form of the experimental signal can be explained using a kinetic scheme (figure 2.4b), which represents processes that occur after excitation of the chromophore to the $S_1^{v=0}$ state. At time zero, the population of the $S_0^{v=v}$ state ≈ 0, and population gain for this state is expected by virtue of stimulated emission from the $S_1^{v=0}$ state. With increasing time, both population gain and loss occurs because both absorption and stimulated emission operate. The larger relative gain near time zero corresponds to a steeper signal decay near time zero (figure 2.5a). However, because of the modulation, the gain and loss signal components are modulated out of phase with respect one another. Therefore, the overall signal which we obtain will appears as the sum of population of gain and loss (Gain – (- Loss) = Gain + Loss, (figure 2.5b)). In this case, there is an apparent buildup (figure 2.5b) rather than fast decay (figure 2.5a) near time zero. The build-up feature contains the T_1 information, while the decay at the longer time contains fluorescence lifetime information. The expression for the detected signal is

$$S(t) \simeq \text{gain} - (-\text{loss}) = \text{gain} + \text{loss} \simeq k\left(\exp(-t/\tau_{S1}) - \frac{T_1}{\tau_{S1}} \exp(-t/T_1) \right) \qquad (2.2)$$

a)

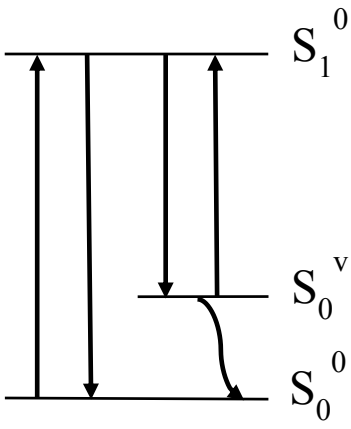

b)

$$S_1^0 \underset{k_{21}}{\overset{k_{12}}{\rightleftarrows}} S_0^v \xrightarrow{k_{23}} S_0^0 \quad \text{(I)}$$

Figure 2.4. a) Three level energy diagram and b) kinetic scheme of dynamic population after excitation to $S_1^{v=0}$.

a).

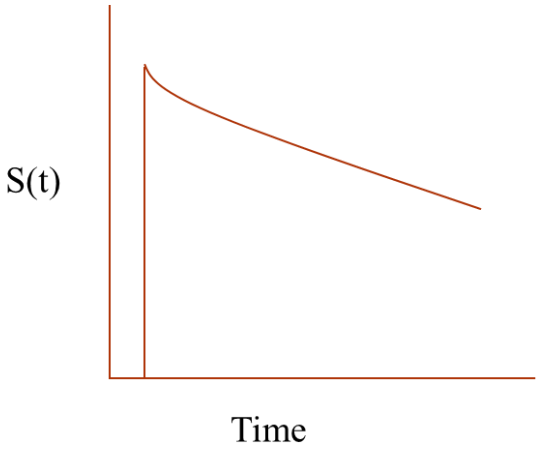

b)

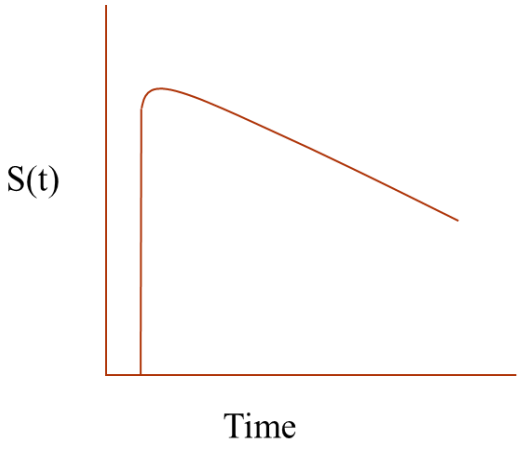

Figure 2.5. a) Difference of population gain from $S_0^{v=\ v} \leftarrow S_1^{v=0}$ stimulated emission and population loss from $S_1^{v=\ 0} \leftarrow S_1^{v=\ v}$ absorption b) sum of population gain from $S_0^{v=\ v} \leftarrow S_1^{v=0}$ stimulated emission and population loss from $S_1^{v=\ 0} \leftarrow S_1^{v=\ v}$ absorption population gain and loss.

where τ_{S1} is the time constant for depopulation of the S_1 electronic state by spontaneous and stimulated emission, and *k* is a scaling factor, typically on the order of 10^{-5}.

2.3 Time-Correlated Single Photon Counting

All of the transient local heating data were obtained by carrying out anisotropy decay measurements with a TCSPC instrument (figure 2.6) that has been described in detail elsewhere.[9] We provide only a brief synopsis of the system here. The source laser for this instrument is a passively mode locked diode pumped Nd:YVO_4 laser (Spectra Physics Vanguard) with the same output parameters as described above for the pump-probe instrument. The third harmonic output of this laser (355 nm) was used to excite a cavity dumped dye laser (Coherent, 702-3, Gooch and Housego cavity dumping electronics) operating with Stilbene 420 laser dye (Exciton Chemical Co.). The dye laser was operated at 437 nm for perylene $S_1 \leftarrow S_0$ excitation (figure 2.7). For $S_2 \leftarrow S_0$ excitation (figure 2.7), the dye laser was operated using Coumarin 480 (Exciton) or Coumarin 490 (Exciton) dyes and was set to 516 nm. The fundamental output of the dye laser was frequency doubled (Inrad, BBO-AC-1, 460 nm-570 nm) to produce 5 ps pulses at 258 nm. For all experiments, a portion of the fundamental excitation pulse is directed to the reference photodiode detector (Becker & Hickl PHD-400-N) while the remainder is directed to the sample. Sample fluorescence is collected perpendicular to the excitation beam axis using a 40x reflecting microscope objective (Ealing). The parallel (vertical, 0°) and perpendicular (horizontal, 90°) emission components are separated using a polarizing cube beam splitter (Newport), and each sent to a detection channel. Each detection channel consists of a subtractive double monochromator(Spectral Products CM-112) and a microchannel plate photomultiplier tube (MCP-PMT, Hamamatsu R3809U-50). The response function for this instrument is typically 35 ps.

Parallel and perpendicular signals are recorded separately by using commercial TCSPC electronics (Becker& Hickl SPC-132) and the data were acquired using a LabVIEW® (National Instruments)

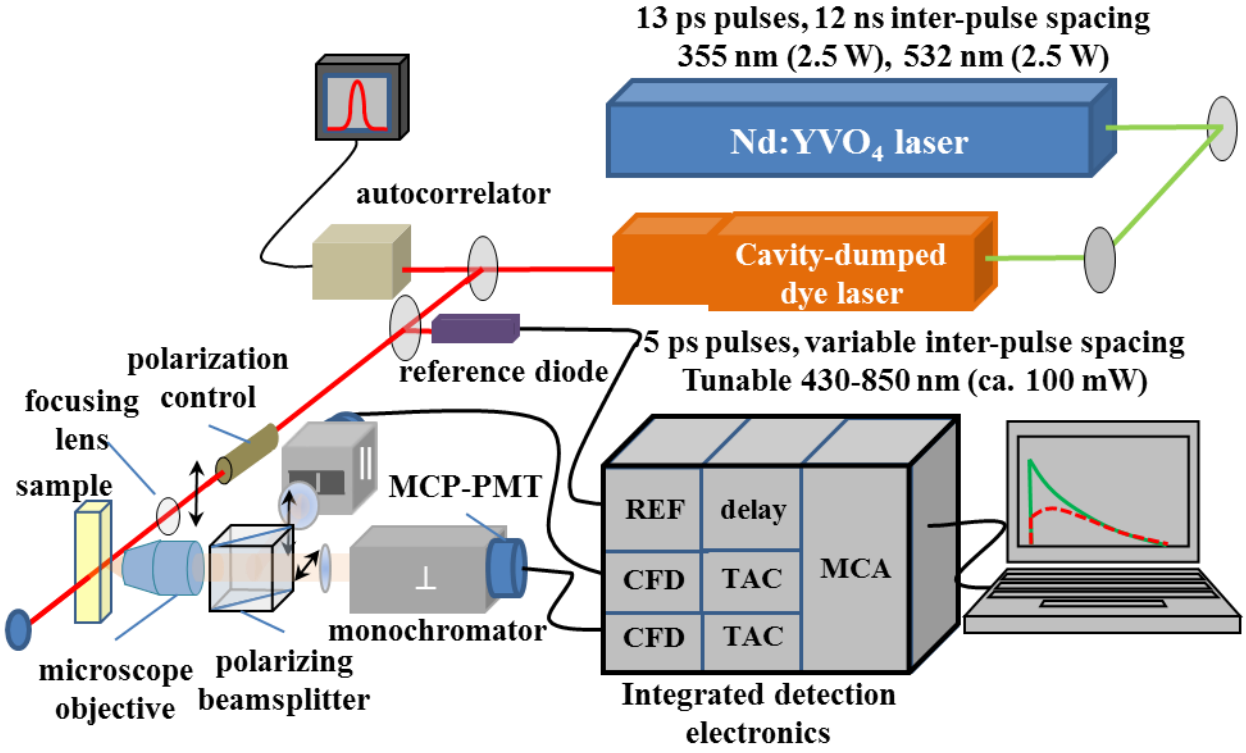

Figure 2.6. TCSPC instrument schematic.

program written in-house and run on a PC. The time window for the sample measurement for the work presented in this thesis is 10000 ps for S_1 excitation and 5000 ps for S_2 excitation. Triplicate measurements were performed for all micelle- and vesicle-containing solutions. The resulting parallel and perpendicular signals can be used to construct the anisotropy decay function, $R(t)$,

$$R(t) = \frac{I_{\parallel}(t) - I_{\perp}(t)}{I_{\parallel}(t) + 2I_{\perp}(t)} \tag{2.3}$$

where $I_{\parallel}(t)$ and $I_{\perp}(t)$ are the polarized emission transients. With these data in hand, the fluidity Local environment of the chromophore and $\boldsymbol{\Delta T}$ can be obtained. The details of the information

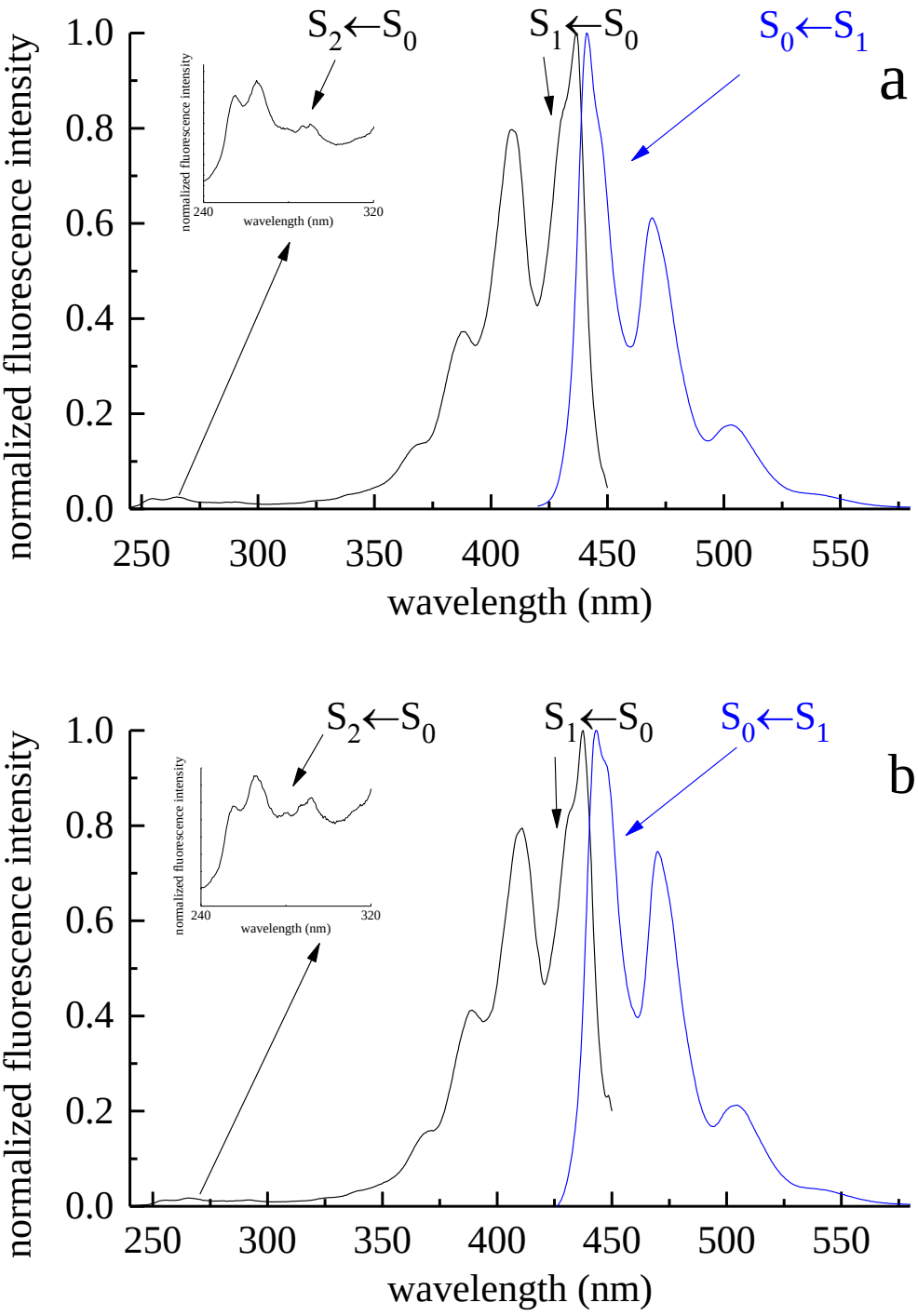

Figure 2.7. Steady state spectra of perylene in (a) decanoate micelles and (b) decanoate / decanoic acid vesicles. Emission is shown in blue and excitation is shown in black.

extracted out from *R*(t) are discussed in detail in chapter 3.

2.4. Dynamic Light Scattering

To measure the size (diameter) of vesicles and micelles, Dynamic Light Scattering (DLS) (Malvern, Zetasizer ZS) also known as photon correlation spectroscopy (PCS) was used. This instrument monitors Brownian motion, the random motion of particles caused by thermal energy. This is done by measuring light scattering from the particles that fluctuates with time. From light intensity fluctuations, the translational diffusion coefficient (D_T) can be obtained using an auto-correlation technique. The D_T quantity then can be related to the hydrodynamic diameter of the particles using the Stokes-Einstein equation (equation 2.4)

$$d\left(H\right) = \frac{k\boldsymbol{T}}{3\pi\eta D_T} \tag{2.4}$$

,where $d(H)$ is the hydrodynamic diameter, D is translational diffusion coefficient, k is Boltzmann's constant, $\boldsymbol{T}$ is temperature, η is viscosity.[10]

REFERENCES

REFERENCES

1. Jiang, Y.; Hambir, S. A.; Blanchard, G. J. *Optics Communications* **1993,** *99* (3–4), 216-220.

2. Jiang, Y.; Blanchard, G. J. *The Journal of Physical Chemistry* **1994,** *98* (38), 9411-9416.

3. Jiang, Y.; Blanchard, G. J. *The Journal of Physical Chemistry* **1995,** *99* (20), 7904-7912.

4. Sala, K.; Kenney-Wallace, G.; Hall, G. *Quantum Electronics, IEEE Journal of* **1980,** *16* (9), 990-996.

5. Bado, P.; Wilson, S. B.; Wilson, K. R. *Review of Scientific Instruments* **1982,** *53* (5), 706-707.

6. Anfinrud, P.; Struve, W. S. *Review of Scientific Instruments* **1986,** *57* (3), 380-383.

7. Andor, L.; Lörincz, A.; Siemion, J.; Smith, D. D.; Rice, S. A. *Review of Scientific Instruments* **1984,** *55* (1), 64-67.

8. Blanchard, G. J.; Wirth, M. J. *Analytical Chemistry* **1986,** *58* (3), 532-535.

9. Pillman, H. A.; Blanchard, G. J. *The Journal of Physical Chemistry B* **2010,** *114* (43), 13703-13709.

10. Skoog, D. A.; Holler, F. J.; Crouch, S. R., *Priciples of Instrumental Analysis*. 6th ed.; Thomson Brooks/ Cole: Belmont, CA, 2007.

Chapter 3: Vibrational Population Relaxation and Transient Heating Data

We report here on two different measurements that relate to the dissipation of energy from a chromophore in molecular environments comprised of the same amphiphiles but with different organization. Measurements of vibrational population relaxation of the perylene 1375 cm^{-1} ring breathing mode sense the initial stage(s) of energy transfer from the molecule excited initially to its immediate surroundings. Measurements of perylene reorientation as a function of excitation energy sense the temperature change of the chromophore immediate environment resulting from the dissipation of excess energy, averaged over the reorientation time of the chromophore. These two types of measurement provide complementary information on the dissipation of energy in solution and how this process depends on the organization of the chromophore local environment. In order to perform these measurements we need to produce both micelles and vesicles of decanoic acid / decanoate amphiphiles and characterize them. We consider this issue before moving on to a discussion of the effects of energy dissipation.

3.1. Sizes of micelles and vesicles

We have used dynamic light scattering to characterize both micelles and vesicles formed using the methods described above. For micelle solutions we recover an average diameter of 2.5 ± 0.5 nm (Figure 3.1a) and for vesicle-containing solutions we observe a bimodal distribution with average diameters of 62 ± 34 nm and 363 ± 40 nm (Figure 3.1b). For the micelles, a simple molecular mechanics calculation of the decanoate chromophore suggests a micelle diameter on the order of 2.7 – 2.8 nm, consistent with the experimental data. The observation of a bimodal distribution for vesicles suggests several possible operative mechanisms for vesicle formation. The distribution centered at 363 nm is determined by the membrane filter pore size used in the extrusion process, and the 62 nm diameter group may be the result of mechanical mixing. It is

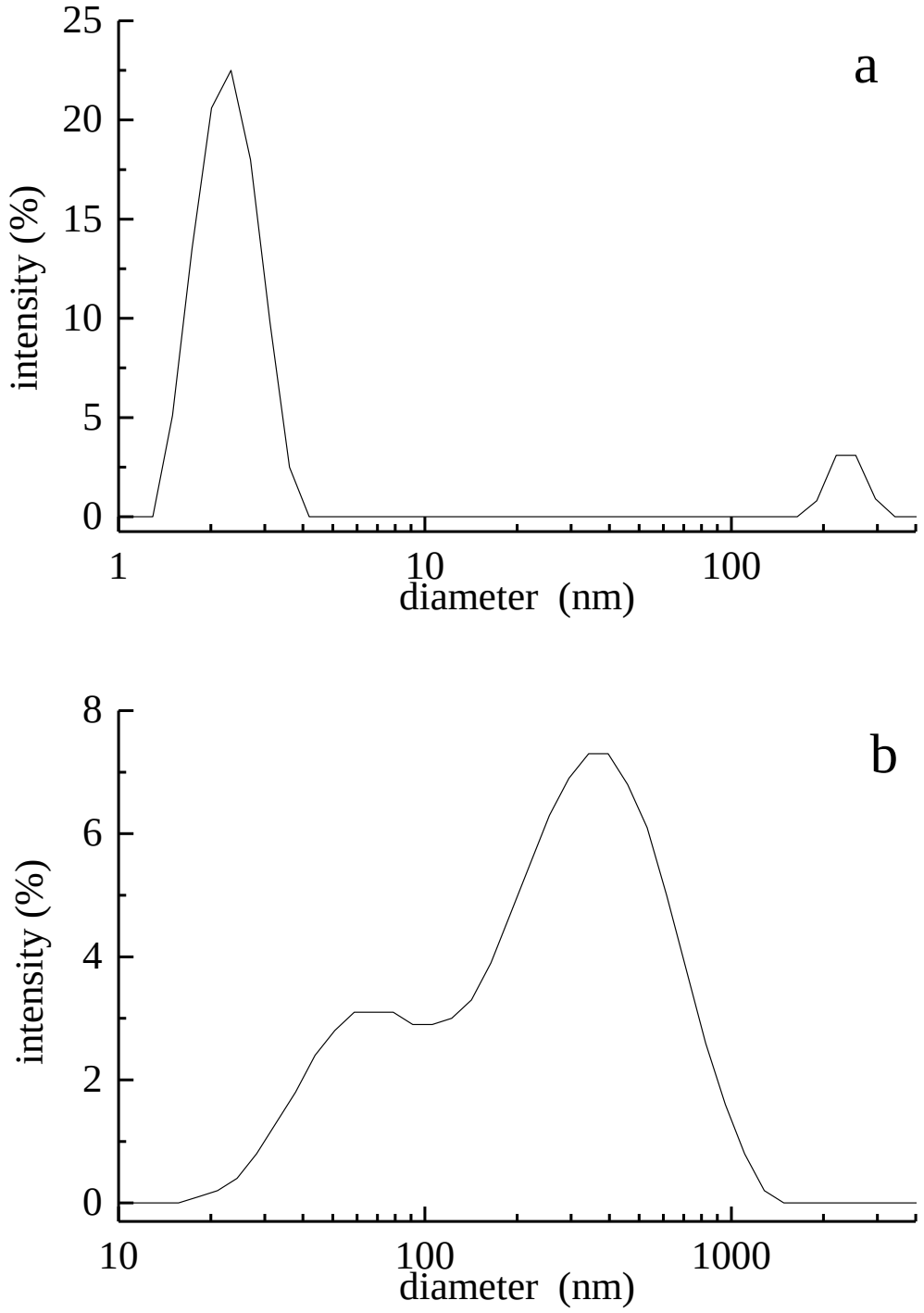

Figure 3.1. Dynamic Light Scattering (DLS) data for aqueous suspensions of (a) micelles (400mM sodium decanoate) and (b) vesicles (400 mM decanoate / decanoic acid).

that the formation of phosphocholine vesicles by sonication leads to vesicles in this same size range.[1] While it is important to know the vesicle size distribution, it is of equal import to note that phospholipid bilayers formed by either sonication or extrusion were characterized by the same molecular-scale organization, as sensed by probe molecular motion.[1]

3.2. *Vibrational Population Relaxation Measurements*

We have measured the vibrational population relaxation time of the perylene 1375 cm^{-1} ring breathing mode in both decanoate micelles and vesicles. This chromophore vibrational mode was chosen because of its energetic proximity to the terminal methyl group rocking mode of the decanoate amphiphile (1378 cm^{-1}), making the energy transfer process resonant. Because perylene possesses a center of inversion, the symmetric ring breathing mode does not modulate any dipole moment, and the coupling between the donor and acceptor modes will scale with r^{-8}.[2] By monitoring T_1, the vibrational population relaxation time constant, of the perylene ring breathing mode as a function of local environment organization, we can gain an understanding of how the perylene local environment and energy transfer efficiency depends on the organization of the medium in which it resides.

The details of the T_1 measurement, using stimulated emission to access donor vibrational modes degenerate with acceptor modes, have been described before.[3-5] The probe molecule is modeled as a coupled three level system, where the three states are the ground state ($S_0^{v=0}$), the ground vibrational state of interest ($S_0^{v=v}$), and electronic excited state ($S_1^{v=0}$). The pump laser beam excites the probe to $S_1^{v=0}$ and the probe laser beam senses the population difference between $S_1^{v=0}$ and $S_0^{v=v}$. Because of the multiple modulation detection scheme used here, the overall detection signal is the sum of contributions from populations in the $S_1^{v=0}$ and $S_0^{v=v}$ states. The signal, $S(t)$, has the functional form

$$S(t) \simeq k\left(\exp(-t/\tau_{S_1}) - \frac{T_1}{\tau_{S_1}} \exp(-t/T_1) \right) \tag{3.1}$$

where τ_{S_1} is the time constant for depopulation of the S_1 electronic state by spontaneous and stimulated emission, and *k* is a scaling factor, typically on the order of 10^{-5}. The data are thus of the form of a signal build-up after time zero (T_1), followed by a monotonic population decay (τ_{S_1}), with the amplitude of the build-up being several percent of the total signal intensity. A representative time-scan is shown in Figure 3.2a and 3.2b.

We found that the time constant, T_1, for energy transfer from the perylene ring breathing mode to the decanoate methyl rocking mode is faster for micelles ($T_1^{\text{micelle}} = 10 \pm 1$ ps) than for vesicles ($T_1^{\text{vesicle}} = 21 \pm 2$ ps). The efficiency of vibrational energy transfer depends on the distance between donor and acceptor and their relative orientations. Because of the spherical shape of micelles, there are more close proximity amphiphile acceptor mode orientations in micelles relative to the orientation of the perylene ring breathing mode than there are in vesicles, and the probability of energy transfer would likely be higher in micelles. In vesicles, perylene is located in the aliphatic chain region, rather than in the inter-leaflet gallery, owing to curvature effects giving rise to asymmetry between the leaflets.[6] Thus, comparatively few amphiphile terminal methyl groups will be in close proximity to perylene in vesicles. In either case, the initial relaxation event for energy flow through the perylene 1375 cm^{-1} ring breathing mode occurs on the 10 – 20 ps timescale. While this process may be somewhat faster or slower, depending on the perylene mode examined, the measured timescale serves as a useful gauge for the initial step in thermal energy dissipation.

3.3. Transient Heating Measurements

Transient local heating measurements of perylene in micelles or vesicles provide

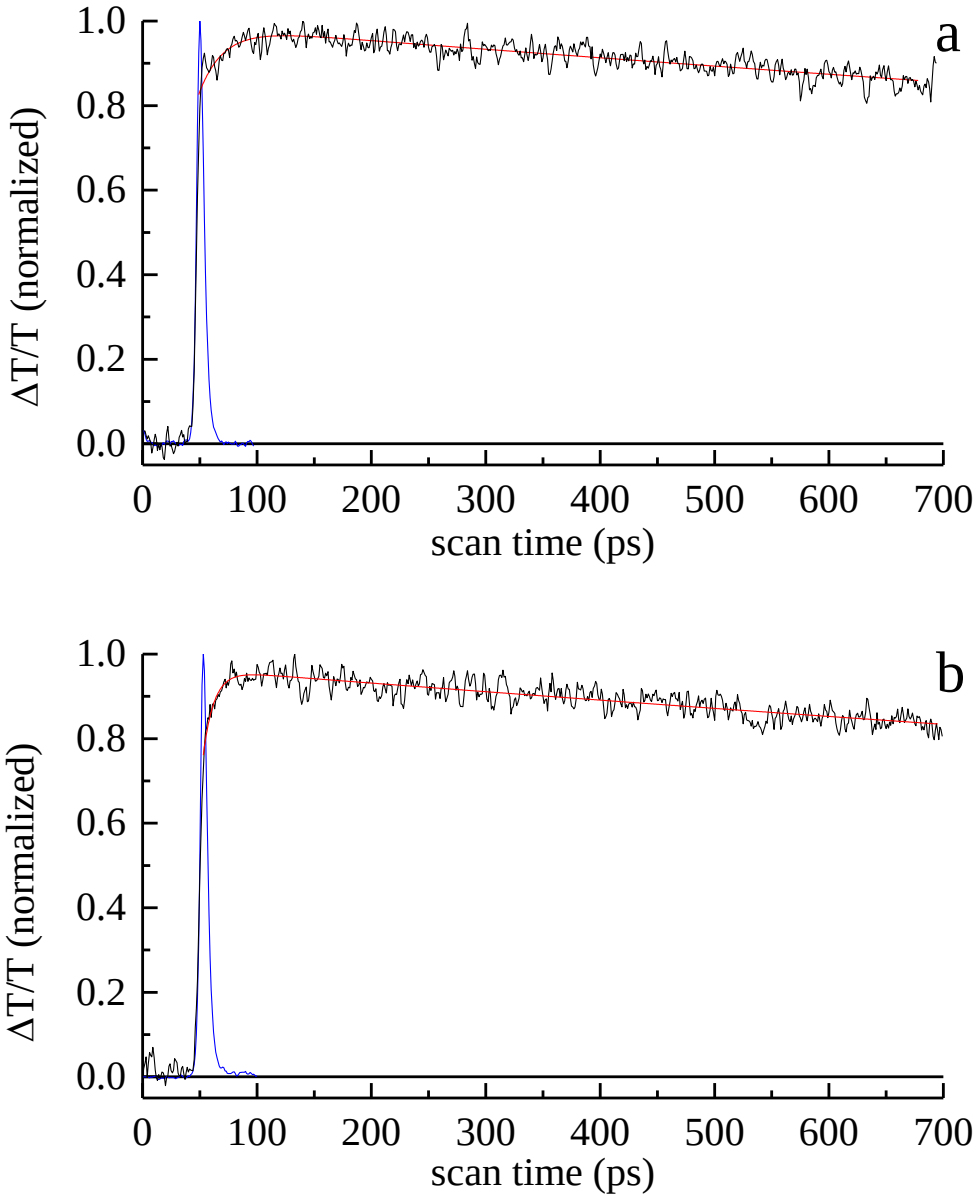

Figure 3.2. The average of three determinations of vibrational population relaxation measurement (probe polarized at 54.7° with respect to pump polarization) of perylene ring breathing mode (1375 cm^{-1}) in (a) decanoate micelles and (b) decanoate / decanoic acid vesicles. The signal is shown in black, the instrument response function is blue, and the fitted decay is red.

information regarding the fate of thermal energy following its deposition into the perylene chromophore. In contrast to the T_1 measurements, which monitor mode-specific relaxation, the measurements we consider next sense non-mode-specific relaxation and monitor the longer-term consequences of thermal energy deposition in micelle and vesicle systems. These measurements thus provide information that is complementary to the T_1 data.

The information extracted from these measurements is in the form of an average temperature change in the system as a result of adding a known amount of excess excitation energy. Perylene is excited to two different electronic states, S_1 and S_2, and the reorientation dynamics of the chromophore are measured using $S_0 \leftarrow S_1$ relaxation for both excitation conditions. Excitation at 437 nm ≈ 2.83 eV ($S_1 \leftarrow S_0$) produces S_1 perylene with little or no excess energy and excitation at 258 nm ≈ 4.81 eV ($S_2 \leftarrow S_0$) produces S_2 perylene with *ca*. 1.98 eV of excess energy. $S_0 \leftarrow S_1$ relaxation is primarily radiative and $S_1 \leftarrow S_2$ relaxation is non-radiative and fast (*ca*. 1 ps). Excitation of perylene to the S_2 state thus provides 1.98 eV of energy that is dissipated to the bath. The thermal energy deposited in the bath results in a temperature jump that dissipates over tens to hundreds of ps, and this change in temperature is sensed as a change in the reorientation dynamics of perylene. It is important to note that the temperature of the local environment is changing continuously after the deposition of excess energy and perylene rotational motion senses the temperature (viscosity) of the local environment averaged over the reorientation time. It is thus not possible to extract quantitative information on the instantaneous jump in temperature upon dissipation of excess energy. Qualitative information, however, is certainly available. We measure the anisotropy decay time constant(s) of perylene in micelles and vesicles under both excitation conditions, extract the viscosity of the chromophore immediate environment, and from that information, estimate $\boldsymbol{\Delta T}$ for micelles and vesicles.[7-10]

For both excitation conditions, the same experimental signal (figure 3.3a, 3.4a, 3.5a, and 3.6a) is used to extract anisotropy decay data. The fluorescence anisotropy decay function, $R(t)$, is given in Eq. 2,

$$R(t) = \frac{I_{\parallel}(t) - I_{\perp}(t)}{I_{\parallel}(t) + 2I_{\perp}(t)} \tag{3.2}$$

Where $I_{\parallel}(t)$ and $I_{\perp}(t)$ are the polarized emission transients. The functional form of $R(t)$ provides the molecular-scale information of interest. $R(t)$ can contain up to five exponential decay components, but typically one or two are seen. Perylene can exhibit either a one- or two-component anisotropy decay, depending on its local environment.[11-14] We observe two exponential decay components for $S_1 \leftarrow S_0$ excitation (figure 3.3b and 3.4b) and one exponential decay component for $S_2 \leftarrow S_0$ excitation (figure 3.5b and 3.6b) for perylene in decanoate micelles and decanoate/ decanoic acid vesicles. The different behavior seen for these two excitation conditions provides significant insight into the details of chromophore molecular motion.

The fluorescence anisotropy decay function can be related to the Cartesian components of rotational diffusion constant, $D = \frac{1}{3}(D_x+D_y+D_z)$ using a treatment reported by Chuang and Eisenthal.[15] For perylene the long in-plane axis is *x*, the short in-plane axis is *y*, and the out of plane axis is *z*. The $S_1 \leftarrow S_0$ transition is *x*-axis polarized and the $S_2 \leftarrow S_0$ transition is *y*-axis polarized in perylene. Because we observe a two-component anisotropy decay for $S_1 \leftarrow S_0$ excitation and a one-component decay for $S_2 \leftarrow S_0$ excitation, it is not sufficient to simply consider perylene reorienting as a prolate or oblate rotor.[15] Rather, a more detailed treatment of perylene reorientation dynamics is required. We have reported and described the details of this treatment before, where perylene can exhibit three possible conditions, designated as rotor Type I, Type II, and Type III.[8]

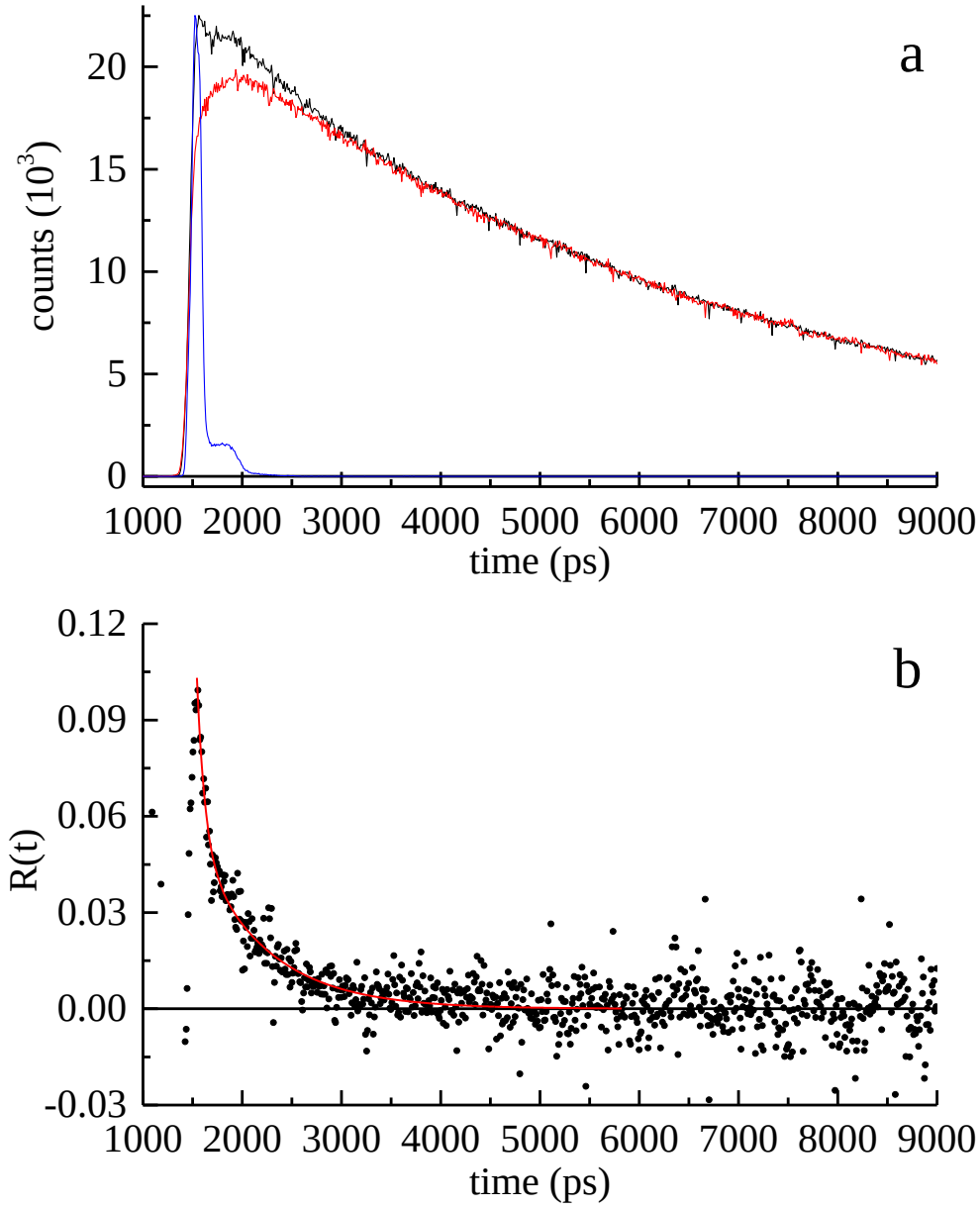

Figure 3.3. (a) Experimental time-resolved polarized fluorescence data for S_1 excitation of perylene in decanoate micelles. $I_{\parallel}(t)$ is black, $I_{\perp}(t)$ is red, and the instrument response function is blue. (b) Anisotropy decay function (black) along with the decay fitting function (red) of perylene in decanoate micelles.

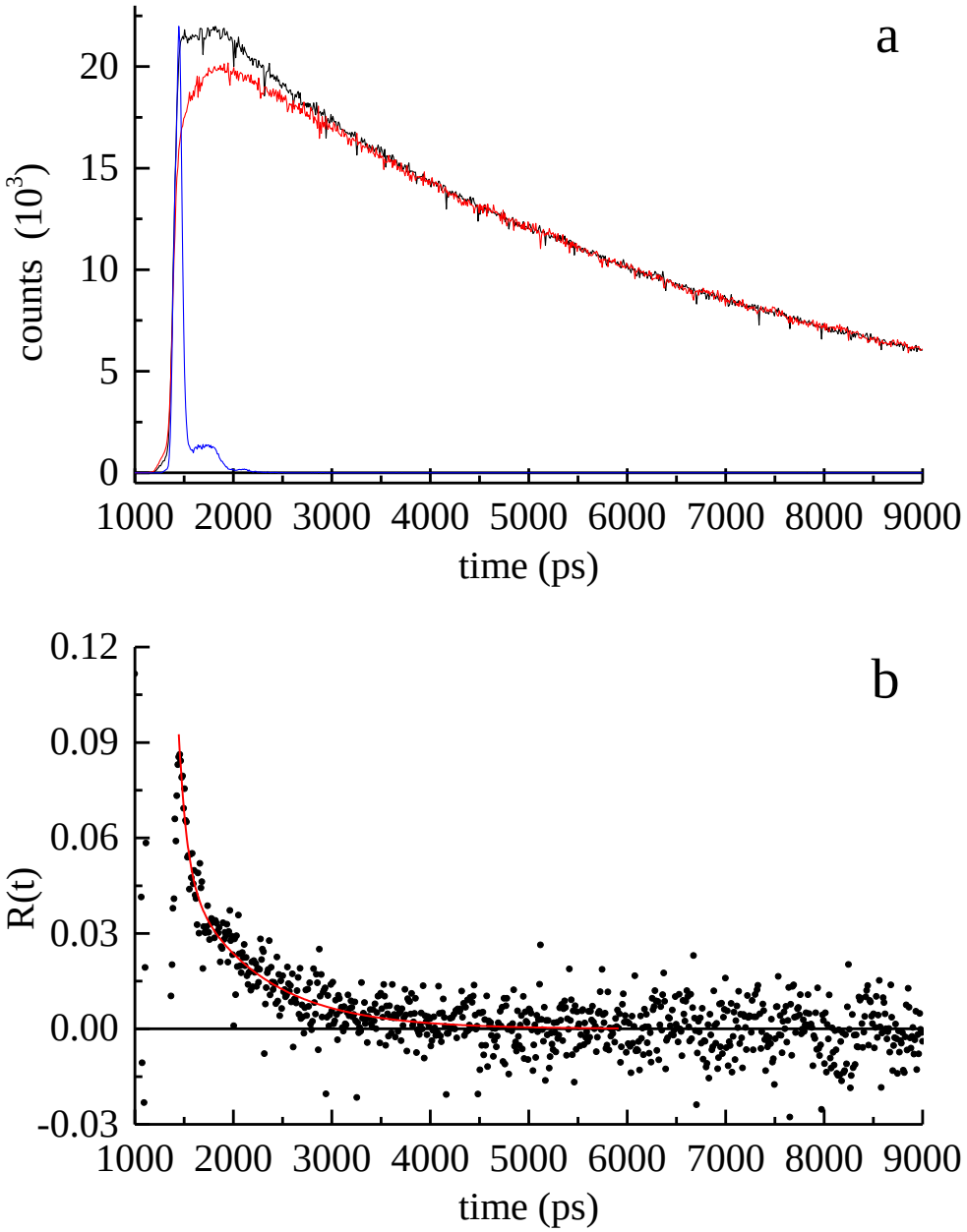

Figure 3.4. (a) Experimental time-resolved polarized fluorescence data for S_1 excitation of perylene in decanoate / decanoic acid vesicles. $I_{\parallel}(t)$ is black, $I_{\perp}(t)$ is red, and the instrument response function is blue. (b) Anisotropy decay function (black) along with the decay fitting function (red) of perylene in decanoate / decanoic acid vesicles.

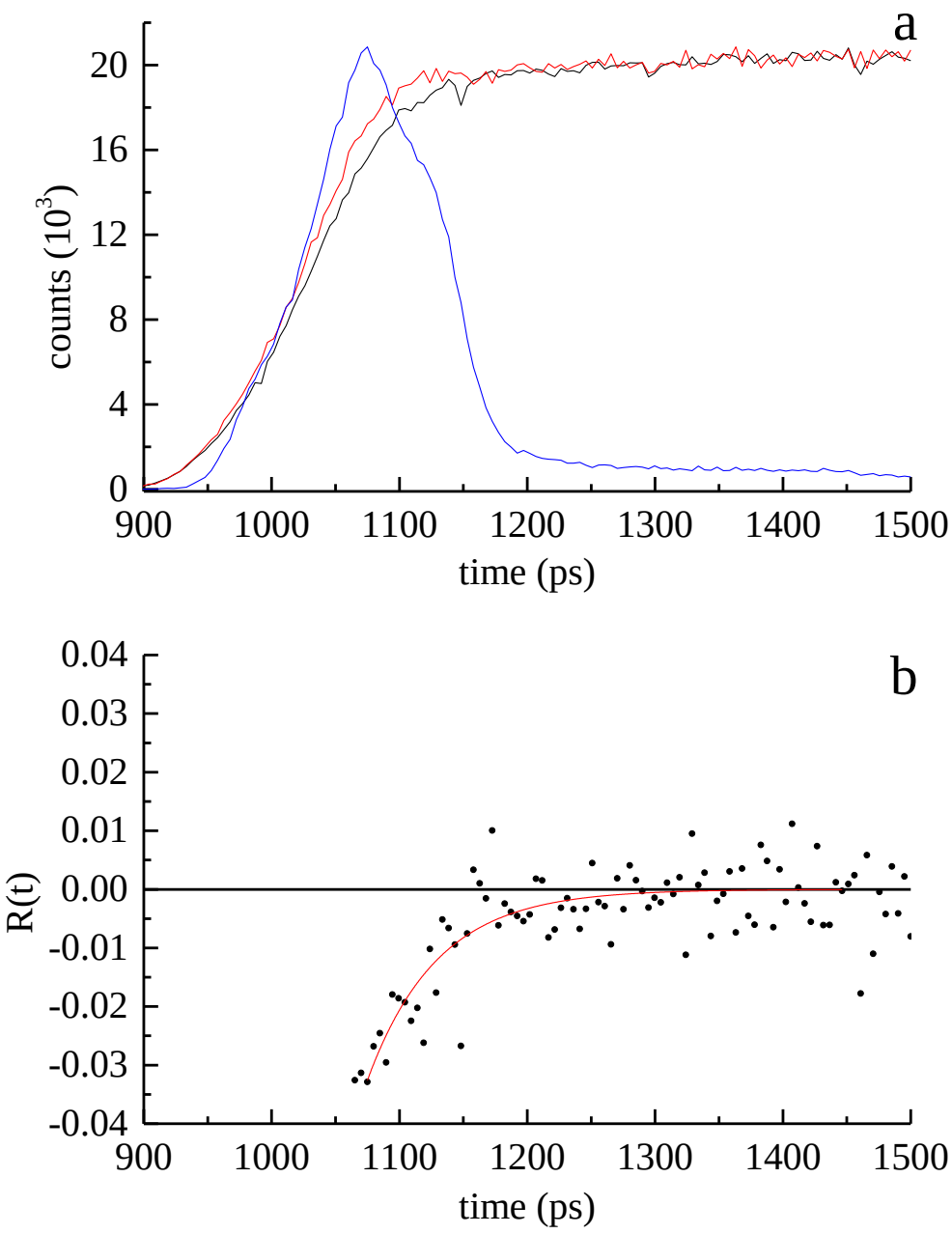

Figure 3.5. (a) Experimental time-resolved polarized fluorescence data for S_2 excitation of perylene in decanoate micelles. $I_{\parallel}(t)$ is black, $I_{\perp}(t)$ is red, and the instrument response function is blue. (b) Anisotropy decay function (black) along with the decay fitting function (red) of perylene in decanoate micelles.

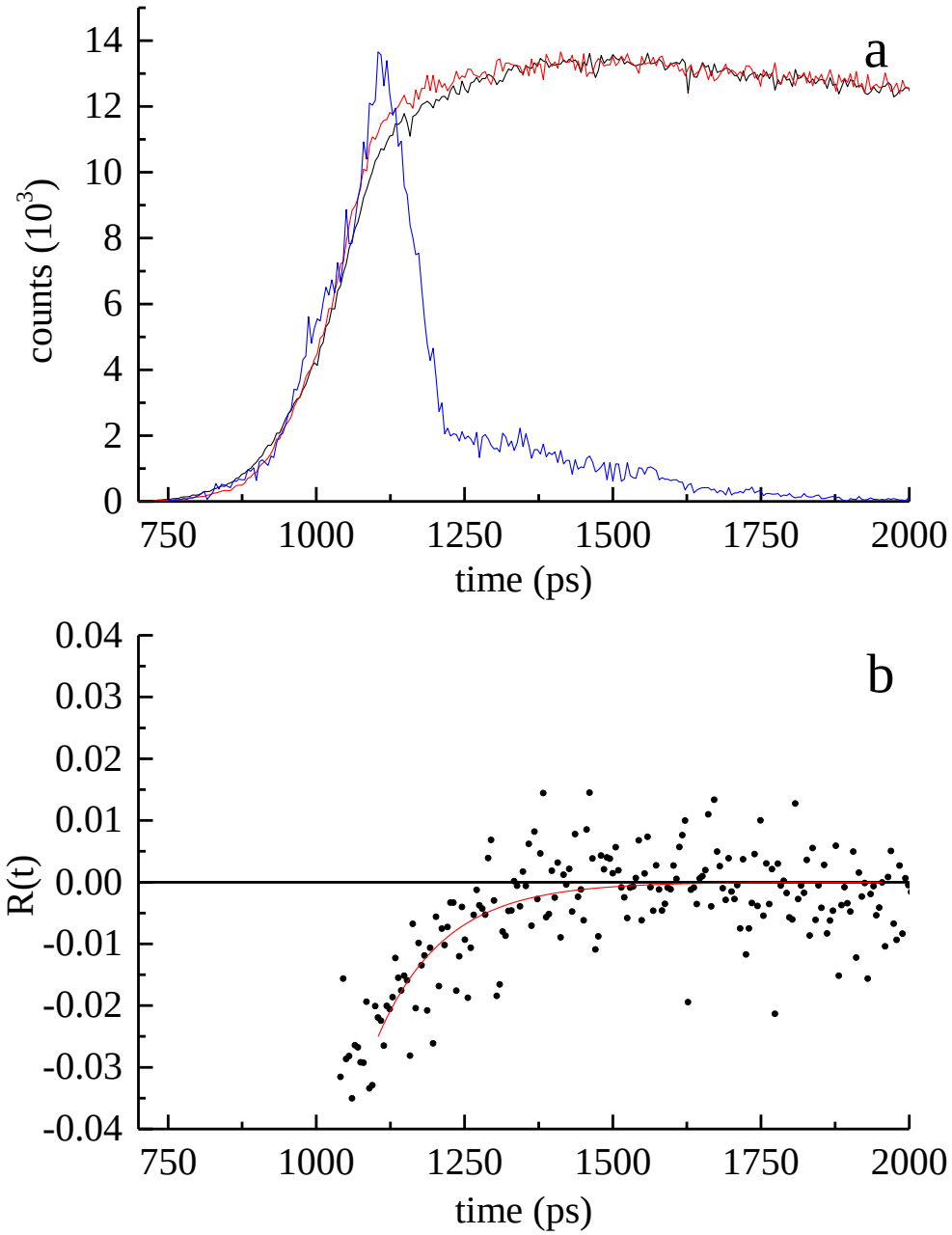

Figure 3.6. (a) Experimental time-resolved polarized fluorescence data for S_2 excitation of perylene in decanoate / decanoic acid vesicles. $I_{\parallel}(t)$ is black, $I_{\perp}(t)$ is red, and the instrument response function is blue. (b) Anisotropy decay function (black) along with the decay fitting function (red) of perylene in decanoate / decanoic acid vesicles.

For perylene, the Type I rotor is defined by having its unique axis of rotation coincide with the excited transition dipole moment. This corresponds to $D_x \neq D_y = D_z$. This condition produces a single exponential decay anisotropy function for both $S_1 \leftarrow S_0$ excitation and $S_2 \leftarrow S_0$ excitation, given by Eqs. 3 and 4, respectively.

$$R(t) = 0.4\exp(-6D_z t) \tag{3.3}$$

$$R(t) = -0.2\exp(-6D_z t) \tag{3.4}$$

A Type II rotor is characterized by the unique rotation axis being perpendicular to the excitation and emission transition dipole moments, $D_z \neq D_x = D_y$. A Type II rotor produces a two component exponential anisotropy decay function for both $S_1 \leftarrow S_0$ and $S_2 \leftarrow S_0$ excitation (Eqs. 3.5 and 3.6, respectively)

$$R(t) = 0.1\exp(-(2D_x + 4D_z)t) + 0.3\exp(-6D_x t) \tag{3.5}$$

$$R(t) = 0.1\exp(-6D_x t) - 0.3\exp(-(2D_x + 4D_z)t) \tag{3.6}$$

For a Type III rotor, $R(t)$ exhibits a double exponential decay for $S_1 \leftarrow S_0$ excitation and a single exponential decay for $S_2 \leftarrow S_0$ excitation.[8] That is the form of our experimental data (Eqs. 3 and 4).

$$R(t) = 0.3\exp(-(4D_y + 2D_z)t) + 0.1\exp(-6D_z t) \tag{3.7}$$

$$R(t) = -0.2\exp(-6D_z t) \tag{3.8}$$

For a Type III rotor, the unique rotational axis is perpendicular to the emission transition dipole moment, but not necessarily perpendicular to the excitation transition dipole moment, $D_y \neq D_x = D_z$.

The experimental decay time constants are related to the Cartesian components of the rotational diffusion constant, D. For $S_1 \leftarrow S_0$ excitation, $\tau_{OR1} = (4D_x + 2D_y)^{-1}$, $\tau_{OR2} = 6D_z^{-1}$ and the

rotor aspect ratio ($D_{major}/ D_{minor} = D_y /D_z$ for Type III) can be determined. For $S_2 \leftarrow S_0$ excitation, $\tau_{OR} = 6D_z^{-1}$. Since there only one Cartesian component (D_z) is available, it is not possible to determine D_y and D_x, but these components can be estimated with the assumption that the aspect ratio of the rotor is the same as it is for $S_1 \leftarrow S_0$ excitation. We recognize that this assumption may not hold quantitatively.

As noted above, we are interested in the change in temperature of the local environment that results from the deposition of excess excitation energy in the chromophore. The temperature change is estimated through the change in viscosity of the local environment. The viscosity of the local environment is related to the rotational diffusion constant, D, through the modified Debye-Stokes-Einstein (DSE) model (Eq. 5).

$$\frac{1}{6D} = \frac{\eta V f}{k_B \boldsymbol{T} S} \tag{3.9}$$

In this model η is the local viscosity, $\boldsymbol{T}$ is the system temperature, k_B is the Boltzmann constant, V is the hydrodynamic volume of the chromophore (225 Å^3 for perylene),[16] S is the shape factor to account for the ellipsoidal shape of the chromophore (0.7),[14, 17] and f is a frictional term that is related to the solvent-solute boundary condition. In the stick limit of strong solvent-solute interactions, $f = 1$, and for nonpolar systems, where weaker solvent-solute frictional interactions are described in the context of the so-called slip limit, $f = 0.0787$ for a shape factor of 0.7.[18] We believe that the slip limit is a more appropriate descriptor of solvent-solute interactions in these systems.

The relationship between system temperature and solvent viscosity is given by the formula,[10,]

$$\boldsymbol{T} = \frac{A}{\eta} - B\eta + C \tag{3.10}$$

where *A*, *B*, and *C* are empirical constants. To obtain $\Delta \boldsymbol{T}$, Eq. 3.11 can be rearranged and differentiated,

$$\frac{\mathrm{d}\eta}{\mathrm{d}\boldsymbol{T}}\Big|_{\boldsymbol{T_0}} = - \frac{\eta^2}{A + \eta^2 B} \tag{3.11}$$

where $\boldsymbol{T_0}$ is the ambient temperature of the decanoate micelle or decanoate / decanoic acid vesicle system and η is the viscosity of decanoic acid in these structures. Decanoic acid is a solid at room temperature and it is not possible to measure the viscosity of these amphiphiles in micelle or vesicle structures directly. Of equal or greater significance is the fact that we cannot measure the temperature-dependence of the system viscosity. The closest liquid phase model is taken to be *n*-decanol, recognizing that this approximation is limited because of the known role of the *n*-decanol hydroxyl functionality in mediating viscosity. The empirical quantities A and B have been determined for *n*-decanol based on temperature-dependent viscosity data (A = 0.9913 K*P, B = 210.8 K/P, $\eta(\boldsymbol{T_0})$ = 0.1105 P),[19-20] and we approximate $\Delta\eta \sim \mathrm{d}\eta$ from our experimental anisotropy decay data to estimate $\Delta T \sim \mathrm{d}T$. We find ΔT for decanoate micelles is 63 ± 3 K and for decanoate / decanoic acid vesicles, ΔT = 53 ± 7 K (Table 3.1).

It is important to consider that the choice of *n*-decanol as a model system for quantitating the viscosity-dependence may play a role in our observations. First, this same model was used for the interpretation of the lipid vesicle data, so those results are directly comparable to those we report here. Second, even if the viscosity of the decanoate micelles or the decanoic acid/decanoate vesicles is substantially different than *n*-decanol, it is the temperature-dependence of the viscosity is of greater importance, and because the aliphatic chain lengths are the same for decanoate and *n*-decanol, we expect the temperature-dependence of the system viscosity to be very similar.

Previous studies of transient local heating effects using perylene in DMPC vesicles or DMPC/cholesterol vesicles found $\Delta \boldsymbol{T}$ to be less than 15 K.[7-8] The $\Delta \boldsymbol{T}$ values we report here are ~

four times higher than those seen for lipid-based vesicles. There are several possible explanations for these findings. The first is that *D* for perylene in decanoate micelles and decanoate / decanoic acid vesicles is faster than in phospholipid vesicles.[7-8] For perylene in DMPC lipid vesicles, *D* is *ca*. 500 MHz ($S_2 \leftarrow S_0$ excitation),[8] and for perylene in decanoate/ decanoic acid vesicles, *D* is *ca*. 8,000 MHz ($S_2 \leftarrow S_0$ excitation, Table 3.1). As noted above, the temperature change sensed by these measurements is the average over the reorientation time, so the shorter the reorientation time, the higher the *D*, and thus, $\Delta \boldsymbol{T}$ will be ($D \propto \Delta \boldsymbol{T}$).[9]

Another potential contribution to our findings is the arrangement of amphiphile head groups at the micelle-water or vesicle-water interface. The headgroup organization of DMPC vesicles will certainly be different than that of the decanoic acid / decanoate vesicles, and this organization may serve to increase the viscosity of the aliphatic chain region. It is also possible that the relaxation of thermal energy from the decanoate micelle and decanoic acid / decanoate vesicle is less efficient than it is lipid vesicles, owing to the greater complexity of the constituent structure and the consequently larger number of degrees of freedom.

We note that the uncertainties in the extracted temperature change in decanoate micelles and decanoate / decanoic acid vesicles overlap at the $\pm 1\sigma$ level. The micelles appear to experience a larger temperature change than the vesicles, on average. If, in fact, this is the case, one possible explanation is that there are more amphiphiles in the vesicle than the micelles, providing more secondary bath modes. In micelles, there are fewer amphiphiles per unit structure, and the finding that these observed $\Delta \boldsymbol{T}$ values are so similar suggests that the relaxation pathway from the amphiphile to the water bath is relatively facile.

$S_1 \leftarrow S_0$ excitation	Micelles	Vesicles
τ_{OR1} (ps)	83 ± 5	73 ± 9
τ_{OR2} (ps)	668 ± 56	758 ± 26
D_{major}/D_{minor} (D_y/D_z)	11.6 ± 0.5	15 ± 1.9
D (MHz)	1130 ± 60	1260 ± 140
η (cP)	23.7 ± 1.2	21.4 ± 2.4

$S_2 \leftarrow S_0$ excitation	Micelles	Vesicles
τ_{OR1} (ps)	56 ± 2	115 ± 11
D_{major}/D_{minor} (D_y/D_z)	11.6 ± 0.5	15 ± 1.9
D (MHz)	13500 ± 1500	8100 ± 1300
η (cP)	2.0 ± 0.2	3.3 ± 0.5
$\Delta\eta$ (cP)	- 21.7 ± 1.2	- 18.1 ± 2.4
ΔT (K)	63 ± 3	53 ± 7

Vibrational population relaxation	Micelles	Vesicles
T_1 (ps)	10 ± 1	21 ± 2
DLS	**Micelles**	**Vesicles**
Size diameter (Peak Location) (nm)	2.5 ± 0.5	363 ± 40 and 62 ± 4
Peak width (nm)	1.0 ± 0.5	189 ± 44^{I} and 34 ± 20^{II}

Table 3.1. Summary of experimental data for micelles (400 mM decanaote) and vesicles (400 mM decanoate / decanoic acid). Note: I). Peak width for 363 nm peak, II). Peak width for 62 nm peak.

REFERENCES

REFERENCES

1. Lapinski, M. M.; Castro-Forero, A.; Greiner, A. J.; Ofoli, R. Y.; Blanchard, G. J. *Langmuir* **2007,** *23*, 11677-11683.

2. Gray, C. G.; Gubbins, K. E., *Theory of Molecular Fluids/ Vol. 1, Fundamentals*. Oxford : Clerendon Press 1984: New York, 1984.

3. Jiang, Y.; Blanchard, G. J. *The Journal of Physical Chemistry* **1994,** *98* (38), 9411-9416.

4. Jiang, Y.; Hambir, S. A.; Blanchard, G. J. *Optics Communications* **1993,** *99* (3–4), 216-220.

5. Blanchard, G. J. *Review of Scientific Instruments* **1996,** *67* (12), 4085-4091.

6. Lapinski, M. M.; Blanchard, G. J. *Chemistry and Physics of Lipids* **2008,** *153* (2), 130-137.

7. Pillman, H. A.; Blanchard, G. J. *The Journal of Physical Chemistry B* **2010,** *114* (43), 13703-13709.

8. Pillman, H. A.; Blanchard, G. J. *The Journal of Physical Chemistry B* **2011,** *115* (14), 3819-3827.

9. Mize, H. E.; Blanchard, G. J. *The Journal of Physical Chemistry B* **2013,** *117* (50), 16260-16265.

10. Dela Cruz, J. L.; Blanchard, G. J. *The Journal of Physical Chemistry A* **2001,** *105* (41), 9328-9335.

11. Christensen, R. L.; Drake, R. C.; Phillips, D. *The Journal of Physical Chemistry* **1986,** *90* (22), 5960-5967.

12. Klein, U. K. A.; Haar, H. P. *Chemical Physics Letters* **1979,** *63* (1), 40-42.

13. Zinsli, P. E. *Chemical Physics* **1977,** *20* (2), 299-309.

14. Jiang, Y.; Blanchard, G. J. *The Journal of Physical Chemistry* **1994,** *98* (26), 6436-6440.

15. Chuang, T. J.; Eisenthal, K. B. *The Journal of Chemical Physics* **1972,** *57* (12), 5094-5097.

16. Edward, J. T. *Journal of Chemical Education* **1970,** *47* (4), 261.

17. Perrin, F. *Journal of Physics Radium* **1936,** *7*, 1.

18. Hu, C. M.; Zwanzig, R. *The Journal of Chemical Physics* **1974,** *60* (11), 4354-4357.

19. Riddick, J. A.; Bunger, W. B.; Sakano, T. K., *Organic Solvents: Physical Properties and Methods of Purification*. Wiley: 1986.

20. Matsuo, S.; Makita, T. *International Journal of Thermophysics* **1989,** *10* (4), 833-843.

Chapter 4: Conclusions and Future Directions

4.1. Conclusions

The ultimate goal of this research was to understand how the assembly or the organization of the molecules affect thermal energy dissipation. Understanding molecular scale energy transfer provides insight on the structural factors influencing processes such as thermal conductivity. Alkanoate amphiphiles were chosen because we can control the local organization of these amphiphiles by changing the pH of the aqueous solution and/ or amphiphile concentration.

We have studied vibrational population relaxation of the perylene ring breathing mode to the amphiphile terminal methyl group rocking mode in decanoate micelles and decanoate / decanoic acid vesicles. The T_1 time is faster in micelles than vesicles by a factor of two, and we understand this effect in terms of the proximity and orientational distribution of acceptor modes being more favorable in micelles. Transient temperature change measurements reveal that the transient temperature change experienced by micelles is slightly higher than it is for vesicles, and we understand this finding in terms of the relative number of relaxation pathways to the bulk system bath for micelles and vesicles. These data provide a self-consistent picture, with early time relaxation events being mediated by the initial donor-acceptor spatial relationship (distance, orientation) and longer-time events being dominated by the total degrees of freedom available for relaxation, once the intrinsic disorder of the amphiphile structures comes into play.

4.2. Future Directions

In this dissertation, only one perylene vibrational mode has been investigated in the initial process of energy transfer. Also, energy can be transferred through the coupling of other perylene vibrational modes to its degenerate or near-degenerate vibrational modes of the amphiphiles. Therefore, in the future, different donor and acceptor vibrational modes coupling need to be

investigated. Other vibrational modes of perylene that are degenerate or near-degenerate with the amphiphiles vibrational modes are listed in table 4.1.

Perylene modes frequency (cm^{-1})	Motion	Decanoate modes frequency (cm^{-1})	Motion	Frequency difference (cm^{-1})
1298	naphthalene rings rocking in plane	1298	CH_2 twisting	0
1141	CH bending	1131	ν_s C-C trans	10
979	symmetric ring deformation	926	accordion CH_2 wag	53
549	asymmetric ring deformation	545	C-C bend	4
357	butterfly mode	343	C-C torsion, with some *g* conformers	14

Table 4.1. Lists of vibrational modes, not all, of perylene and its degeneracy to the decanoate vibrational modes.

Another future direction of this research should be the vibrational population relaxation and anisotropy measurement of perylene as a function of decanoate / decanoic acid vesicles size. This approach is useful to understand energy transfer as a function of local environment, and bilayer curvature. As the size of the vesicles increases, the curvature decreases leading to a more planar-like bilayer structure. For phospholipids, curvature was shown to be important in determining the location of the chromophore within the nonpolar region.[1]

Another future direction of this research is to employ probe molecule that doesn't possess center of inversion. In this case, 1-methylperylene is a good candidate because of its structure similarity to perylene, it is well studied, and it partitions into the nonpolar region of decanoate micelles or decanoate / decanoic acid vesicles.[2-5] The use of 1-methylperylene will allow us to investigate intermolecular VET over longer intermolecular distance scale because it will couple with the amphiphile acceptor modes through dipole-dipole interactions, which scale with r^{-6}.[6]

Another future direction that can be pursued is the use of tetracene as a probe molecule in the decanoate system as a comparison with the perylene in decanoate system. Tetracene, like perylene, possesses a center of inversion, meaning that all Raman-active mode will couple to

a b

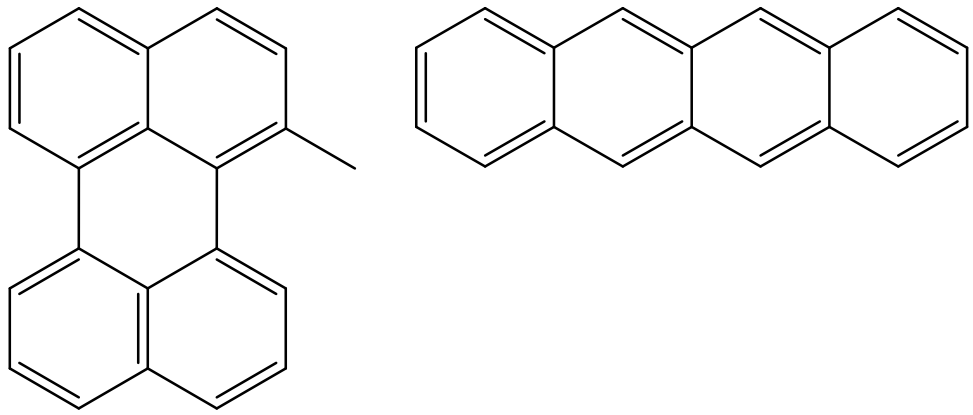

Figure 4.1. Structure of a) 1-methylperylene and b) tetracene.

acceptor modes with r^{-8} or r^{-10} distance dependencies.[6] The use of tetracene as a probe molecule provides insight on the effects of probe molecular structure on the flow of energy. By evaluating different structural aspects of energy dissipation processes, we anticipate that a larger sense of the molecular factors that determine thermal conductivity will become clearer.

REFERENCES

REFERENCES

1. Lapinski, M. M.; Blanchard, G. J. *Chemistry and Physics of Lipids* **2008,** *153* (2), 130-137.

2. Goldie, S. N.; Blanchard, G. J. *The Journal of Physical Chemistry A* **1999,** *103* (8), 999-1006.

3. Goldie, S. N.; Blanchard, G. J. *The Journal of Physical Chemistry A* **2001,** *105* (28), 6785-6793.

4. Jiang, Y.; Blanchard, G. J. *The Journal of Physical Chemistry* **1995,** *99* (20), 7904-7912.

5. McCarthy, P. K.; Blanchard, G. J. *The Journal of Physical Chemistry* **1996,** *100* (13), 5182-5187.

6. Gray, C. G.; Gubbins, K. E., *Theory of Molecular Fluids/ Vol. 1, Fundamentals*. Oxford : Clerendon Press 1984: New York, 1984.